

Non-coherent Detection and Bit Error Rate for an Ambient Backscatter Link in Time-Selective Fading

J. Kartheek Devineni and Harpreet S. Dhillon

Abstract

This paper is focused on the non-coherent detection in ambient backscatter communication, which is highly appealing for systems where the trade-off between signaling overhead and the actual data transmission is very critical. Modeling the time-selective fading channel as a first-order autoregressive (AR) process, we consider two data encoding schemes at the transmitter and propose a new receiver architecture based on the direct averaging of the received signal samples for detection, which departs significantly from the energy averaging-based receivers considered in the literature. For the proposed setup, we characterize the exact asymptotic bit error rate (BER) for both single and multi antenna receivers. Our results demonstrate that while the direct interference received from the ambient power source leads to a BER floor in the single antenna receiver, the multi-antenna receiver can efficiently remove this interference by estimating the angle of arrival (AoA) of the direct link from the power source. A key intermediate result of our analysis is a new concentration result for a general sum sequence (including the asymptotic growth rates of its expectation and variance) that is central to the derivation of the conditional distributions of the signal at the receiver.

Index Terms

Ambient backscatter, non-coherent detection, auto-regressive model, time-selective fading, bit error rate.

I. INTRODUCTION

Ambient backscatter with its technological capability to support battery-free communication has shown remarkable potential in enabling information transfer among energy-constrained de-

J. K. Devineni and H. S. Dhillon are with Wireless@VT, Department of ECE, Virginia Tech, Blacksburg, VA (email: kartheekdj@vt.edu and hdhillon@vt.edu). This work was supported by U.S. NSF under Grant CPS-1739642. This work will be presented in part at the IEEE Globecom, Waikoloa, HI, 2019 [1].

Manuscript updated: January 27, 2023.

vices within the Internet-of-Things (IoT) paradigm [2]–[4]. Given the diverse nature of applications envisioned in the IoT ecosystem, the channel conditions experienced by the IoT devices across different applications could vary significantly [5]. In the context of this paper, the channel coherence time experienced by these devices could vary by orders of magnitude across applications. For instance, IoT devices deployed in high mobility scenarios, such as vehicles, road signs, or traffic posts, are expected to experience higher Doppler spread, and hence lower channel coherence time, compared to the IoT devices deployed in relatively static scenarios, such as homes, offices, and public places. While the latter case has implicitly been the focus of most of the prior work on ambient backscatter communication systems, the former is equally, if not more, important but has not received much attention. Most notably, lower coherence time makes it difficult to implement channel estimation and tracking procedure using either training or blind estimation. Because of this, one needs to consider non-coherent detection schemes for such scenarios, which have not yet been investigated in the context of ambient backscatter communications. Motivated by this knowledge gap, this paper focuses on receiver design, encoding schemes, and comprehensive performance characterization of non-coherent detection-based ambient backscatter system under time-selective fading channels.

A. Related Work

As noted above, the existing literature on ambient backscatter is mainly focused on the slow fading channels that assume a block fading model [6]–[22]. Maximum-likelihood (ML) detection under an ambient backscatter setup was first investigated in [7]. The signal detection under non-coherent and semi-coherent setups is analyzed in [8]–[11]. The signal detection at a multi-antenna receiver is studied in [12] and the statistical-covariance based detection is explored in [13]. While [6]–[12] were based on the Gaussian distribution approximation for the conditional distributions of the average energy of the received signal, the exact BER analysis for the slow fading case was performed in [5]. Interested readers can also refer to [5] for a detailed overview of the backscatter concept. Ambient backscatter communication using orthogonal frequency division multiplexing (OFDM) is investigated in [14], [15]. On the same lines, [16], [17] explored new coding schemes, such as Manchester coding, to improve detection performance.

A general requirement of coherent detection is the transmission of pilot/training symbols from transmitter to receiver nodes for the estimation of channel state information. This will require some form of cooperation between the primary and backscatter network nodes which

might not always be possible. Hence, alternate approaches that avoid the transmission of pilots, such as blind channel estimation techniques, have also been investigated for ambient backscatter [18]–[22]. These approaches use different techniques from Bayesian statistics such as expectation-maximization (EM) or space alternating generalized expectation-maximization (SAGE) to iteratively implement the maximum *a posteriori* probability (MAP) or ML methods to perform the channel estimation from the received signal directly. The performance of these techniques depends on the accuracy and the convergence rate of the blind channel estimation procedures. Therefore, if the convergence rate is slow, these techniques might not be suitable for implementation in a time-selective fading channel. We overcome this drawback by investigating a non-coherent detection technique that only requires estimating large-scale parameters, such as AoA.

B. Contributions

To the best of our knowledge, this is the first work that presents a comprehensive analytical treatment of non-coherent detection for ambient backscatter under a time-selective fading channel. We analyze two types of receivers for this setup: 1) single antenna receiver, and 2) multi-antenna receiver. The number of antennas in the multi-antenna receiver are assumed to be two. A binary hypothesis testing problem is formulated for the transmission of binary message data. In addition, two data encoding schemes are used at the transmitter, in which the first one directly transmits the message bit using on-off keying (OOK) modulation, and the second one transmits codewords [0 1] and [1 0] for the message bit using OOK modulation over two symbol durations.

New Receiver Architecture: As noted above already, the prior work on ambient backscatter communication has mainly focused on coherent and and semi-coherent detection techniques. In all these works, the receiver architecture is based on computing the average energy of the received signal samples. It is natural to wonder whether one can use simpler architecture based on direct averaging of the received signal samples, which would reduce the complexity of the receiver. Unfortunately, under the above techniques, this simpler detector results in similar conditional distributions for different hypotheses, which makes it harder to differentiate the transmitted backscatter signal. However, for the non-coherent detection, both architectures result in similar conditional distributions under different hypotheses since the channel coefficients are unknown. The one based on the energy averaging requires two additional operations of computing the

magnitude and squaring on each signal sample, which makes it relatively more complex. Besides, it is less tractable as evaluation of the expressions for optimal detection strategies in this detector is not easy [6]. Due to these reasons, we employ the receiver architecture based on the direct averaging of the received signal samples in this work. By deriving BER for the non-coherent setup, we concretely demonstrate that while the new architecture is inadequate for a single antenna receiver in an ambient backscatter system, it results in dissimilar conditional distributions when used in conjunction with a multi-antenna receiver, which is attributed to the elimination of the strong interference generated by the direct link from the power source. The novelty of the multi-antenna receiver designed here lies in its ability to exploit the fact that the time-scale over which AoA varies is much larger than the time-scale over which the overall channel gain varies and use it for tracking the AoA of the direct link. As implied already, the new receiver architecture also results in tractable conditional distributions, which facilitates the derivation of the optimal detection strategies and the evaluation of the exact BER.

Asymptotic Growth Rate of a Generalized Sum Sequence: During the process of deriving conditional distributions for the null and alternate hypotheses, we come across a generalized sum sequence with correlated samples. We investigate the asymptotic growth rate of this sum sequence and use it to derive a new concentration result for another specific sequence of interest. This contribution is central to the evaluation of the exact asymptotic conditional distributions and is also fundamental to the subsequent BER analysis.

Insights: Our analysis has shown that the single antenna receiver quickly reaches a BER floor due to the strong interference from the ambient power source. The performance can be drastically improved by using the multi-antenna receiver to track the AoA of the direct link, and cancel the strong interference coming from the power source. Further, BER with the new receiver architecture is independent of the signal sample-size of the averaging operation for some cases, such as zero expected value of the ambient data sequence and/or uncorrelated time-domain fading. For the more general case of correlated fading, the BER reaches an asymptotic value due to the diminishing returns in the BER improvement with increasing sample size. Further, the BER is observed to improve with increasing time-domain correlation of the fading channel.

II. SYSTEM MODEL

A. Channel Model

We consider a spatially correlated flat Rayleigh fading channel with coherence time of the order of the symbol duration of the ambient RF data, which corresponds to a fast fading scenario. The impulse response of this channel can be expressed in terms of the dominant NLOS path and the receiver antenna array response as follows:

$$\vec{h}(t) = \underbrace{\sum_{n=1}^N c_n e^{j\phi_n - j2\pi c \tau_n / \lambda + j2\pi f_d \cos \psi_n t}}_{h_0(t)} \vec{a}(\theta_0) \delta(t - \bar{\tau}), \quad (1)$$

where the dominant NLOS path can be assumed to be a combination of N independent sub-paths due to the presence of local scatterers around the transmitter. The n th sub-path is characterized by the gain c_n , the phase offset ϕ_n , the time delay τ_n , the maximum Doppler spread f_d , and the angle of departure (AoD) ψ_n at the transmitter, as given in the equation. The remaining parameters $\vec{a}(.)$ and θ_0 are the antenna array response vector of the receiver and the AoA of the NLOS path, respectively. The phase offset ϕ_n of each sub-path is uniformly distributed over $[0, 2\pi)$, and the additional phase offset resulting from the path-delay τ_n can also be shown to be uniformly distributed over $[0, 2\pi)$ since the frequency of operation is very high [23, Lemma 4]. The envelope of the resulting channel coefficient $h_0(t)$ can be characterized as a Rayleigh distributed random variable (RV) by invoking the central limit theorem (CLT) for the independent sub-paths. This channel environment is illustrated in Fig. 1. The described channel environment is close to many real-world scenarios, and in the case of ambient backscatter it corresponds to the scenario where a moving mobile user is used as a power source by a transmitter to communicate with a receiver which can be either a base station (BS) or another backscatter device.

The rate at which the coefficient $h_0(t)$ varies is dependent on the maximum Doppler spread f_d and the angular spread ψ_n of the sub-paths at the mobile user. These parameters are large enough in this case due to the movement of the user and the presence of local scatterers, resulting in a fast variation of $h_0(t)$. On the other hand, the array response vector $\vec{a}(.)$ depends on the AoA θ_0 of the NLOS path. The time-scale over which this parameter θ_0 evolves is several orders of magnitude larger compared to the coherence time of $h_0(t)$, and hence can be tracked by the system. Therefore, while the channel coefficient at the receiver will be changing for each ambient symbol, the angular variation corresponding to AoA of the received signal will not change at

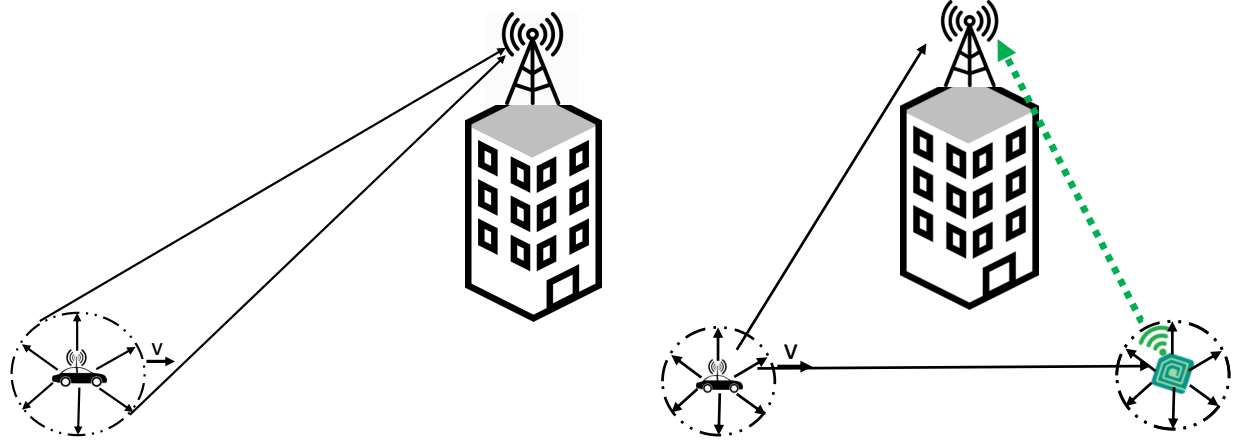


Fig. 1: Illustration of the time-selective fading channel. **Fig. 2:** System model for the ambient backscatter setup.

the same rate and can be assumed to be constant for few symbol periods. The multi-antenna receiver designed in this work will build on this point to improve the BER performance of the system. More information on this channel model can be found in [24]–[26].

Remark 1. *The assumption of spatially correlated channel at the receiver is typically valid for a BS located above the rooftops as the angular spread is small in these scenarios. We assume this to be valid for a backscatter device too by considering a single dominant NLOS path. Handling the case of multiple angular paths at the receiver is left as a promising future work.*

The auto-correlation function characterizes the second order statistics of this fading process and can be derived as follows:

$$\mathbb{E}_{\theta_n, \tau_n, \bar{\psi}} [h_0(t)h_0^*(t + \tau)] = \left(\sum_{n=1}^N |c_n|^2 \right) \mathbb{E}_{\bar{\psi}} \left[e^{-j2\pi f_d \cos \bar{\psi} \tau} \right] = \left(\sum_{n=1}^N |c_n|^2 \right) J_0(2\pi f_d \tau), \quad (2)$$

where $J_0(\cdot)$ is the zero order Bessel function of the first kind. This result, known as Jakes model, is obtained by assuming that the departure angle is uniformly distributed over the azimuthal space.

Autoregressive (AR) Modeling of Fading Channels: The Jakes model that was described above for the temporal-fading process is one of the most widely used statistical channel models in the literature. However, this approach is not always convenient to apply for procedures such as channel modeling, estimation and equalization. Instead, AR models are used in these cases either to decrease complexity in generating accurate correlated samples of this time-domain fading process or for easier derivation of the channel equalization parameters [27]–[30]. Therefore, to simplify the analysis, the time-selective fading channel in our work is also modeled as an AR

process. The correlation matching (CM) criterion of the AR model imposes a condition that the auto-correlation function (ACF) of the approximated discrete process should match the sampled ACF of the Jakes model. An AR process of order p is given by [27]:

$$h(n) = \sum_{k=1}^p a_k h(n-k) + v(n), \quad (3)$$

where $v(n)$ is a complex white Gaussian noise process with uncorrelated real and imaginary components. In the case of Rayleigh fading, $v(n)$ has zero mean. The parameters related to the AR model are given by $\{a_1, a_2, \dots, a_p\}$ and the variance of $v(n)$ by σ_p^2 . The ACF of this approximated process of order p matches exactly with the samples of the desired ACF upto p taps. The accuracy of this modeling approach using AR process increases with higher order approximations. However, as shown in [31], the first order AR model obtained by setting $p = 1$ is a sufficiently accurate model which can be represented as [28]:

$$h(n) = \rho h(n-1) + \sqrt{1-\rho^2} g(n), \quad (4)$$

where $h(n)$ and $h(n-1)$ are the channel gains in the current and previous time periods, $g(n)$ is the complex white Gaussian noise process with variance σ_h^2 , and $\rho = J_0(2\pi f_d T_s)$ is the correlation between fading coefficients of the consecutive symbols which is given in terms of the zeroth order Bessel function J_0 , the symbol duration T_s , and the Doppler spread f_d . The time-selective fading channel is modeled by the correlation factor $\rho \in [0, 1)$ and the value of ρ determines the rate at which the current channel coefficient de-correlates with the previous coefficients. The recursive relation in (4) can be expanded and written in the direct form as below:

$$h(n) = \rho^{n-1} h(1) + \sqrt{1-\rho^2} \left\{ \sum_{k=1}^{n-1} \rho^{n-k-1} g(k) \right\}. \quad (5)$$

Remark 2. *The analysis for the time-selective fading channel implicitly handles the two extreme cases of independent fading ($\rho = 0$) and highly correlated fading ($\lim \rho \rightarrow 1^-$). However, the block fading channel modeled by configuring $\rho = 1$ requires a separate analysis and hence, will be handled separately in a future work.*

B. Signal Model

The ambient backscatter setup considered in this paper consists of three devices: ambient power source, backscatter transmitter (BTx), and receiver (Rx), as illustrated in Fig. 2. The ambient power source is assumed to be a single antenna transmitter. However, even if multiple

antennas are used, for example to beamform the signal, it would only change the power gain at the receiver. The power gain is a function of the antenna array factor and the angular position of the backscatter transmitter-receiver pair, where the gain either increases or decreases depending on whether the pair is located either inside or outside the angular zone of the intended receiver, respectively. This would not affect our analysis since the power gain of the signal is a large-scale parameter which would be absorbed into the signal to noise ratio (SNR) of the ambient signal. At the receiver, the signal scattered from the backscatter device is given by [32]:

$$r = (A - \Gamma) s = As - \Gamma s, \quad (6)$$

where r is the signal at the receiver, s is the signal backscattered at the device, A is the load-independent complex coefficient of the device, and Γ is the reflection coefficient of backscatter node at the boundary of the antenna and the circuit. The device modulates the signal by varying the load impedance to change the parameter Γ that controls the reflected signal. The first and second terms in (6) correspond to the *structural mode* and *antenna mode* scattering components. A binary modulation scheme can be implemented by choosing two different values Γ_0 and Γ_1 . As will be shown later in the analysis, the non-coherent detection will result in good performance exclusively for the case of OOK modulation. It is possible to achieve this modulation for antennas with $|A| \leq 1$ by designing the appropriate load impedance using only passive components such as resistors, capacitors, and inductors [33], [34].

We assume that the rate of backscatter data is significantly lower than the rate of ambient radio frequency (RF) data which is reasonable for most IoT applications. This allows us to represent the backscatter data as a single variable b for a block of received signal samples, whose size is denoted by N . For an Rx with single antenna, the received signal is composed of two components, one directly received from the power source and the other reflected from the BTx. This can be mathematically represented as follows:

$$y(n) = \underbrace{h_r(n)x(n)}_{\text{direct signal}} + \underbrace{\alpha b h_b(n) h_t(n)x(n)}_{\text{backscatter signal}} + \underbrace{w(n)}_{\text{AWGN}}, \quad (7)$$

where $x(n)$ is the ambient radio signal in complex baseband form, $w(n)$ is the additive complex Gaussian noise, $h_r(n)$, $h_b(n)$ and $h_t(n)$ are zero mean complex Gaussian channel coefficients with a variance of σ_h^2 , $b \in \{0, 1\}$ is the backscatter data and α is related to the parameter Γ_1 of the BTx node. Since the non-coherent receiver does not estimate the channel state information, the channel coefficients $h_r(n)$, $h_b(n)$ and $h_t(n)$ are unknown to it. We assume that the BTx uses

a simple binary on-off modulation scheme to transmit the digital data. This received signal can be easily modified for a two antenna Rx as follows:

$$\mathbf{y}(n) = \begin{bmatrix} y_0(n) \\ y_1(n) \end{bmatrix} = h_r(n) \begin{bmatrix} 1 \\ e^{j\phi_1} \end{bmatrix} x(n) + ab h_b(n) h_t(n) \begin{bmatrix} 1 \\ e^{j\phi_2} \end{bmatrix} x(n) + \begin{bmatrix} w_0(n) \\ w_1(n) \end{bmatrix}, \quad (8)$$

where $\phi_i \equiv \frac{2\pi}{\lambda} d \cos \theta_i$ is the phase offset between the two antennas which is dependent on AoA θ_i . Note that the AoA θ_2 of the backscatter link is independent of the AoA θ_1 of the direct link.

The null and alternate hypotheses of the binary hypothesis testing problem are denoted as \mathcal{H}_0 and \mathcal{H}_1 , respectively. In the first encoding scheme, denoted as \mathcal{M}_1 , the message bit is directly transmitted using on-off keying (OOK) modulation, while in the second scheme, denoted as \mathcal{M}_2 , codewords [0 1] and [1 0] are transmitted for the message bit using OOK modulation over two symbol durations. The encoding used in \mathcal{M}_2 is one of the standard schemes used for non-coherent detection in the literature [35]. The receiver architecture is based on the mean of the received signal samples which is given by $Y = \frac{1}{N} \sum_{n=1}^N y(n)$. As is generally the case, the ambient data symbols $x(n)$ are assumed to be an independent and identically distributed (i.i.d.) sequence.

III. DETECTION AT A SINGLE ANTENNA RECEIVER

In this section, we initially derive the growth rate of the expectation and variance of the generalized sum sequence of interest. This result is then used to evaluate the conditional distributions of the signal of the two hypotheses under the two encoding schemes. Using these results, the BER of the two encoding schemes for the single antenna receiver are determined.

A. Growth Rate of a Generalized Sum Sequence of Interest

Consider the general sum sequence $S_N = \sum_{n_1, n_2} \rho^{|n_1 - n_2|} x(n_1) x^*(n_2)$, defined as the sum of non-i.i.d. RVs, which plays an important role in the signal detection procedure. In particular, the asymptotic property of the sum sequence given by $M_N = \frac{S_N}{N}$ is required to derive the conditional distributions. For this setup, if we can show that the growth rate of both the expectation and variance of S_N is of the order of N (the number of samples), that is sufficient to conclude that the sequence M_N converges to its mean value as the sample size tends to infinity. Using the Chebyshev inequality, it is possible to show that this will indeed be the case if the higher order moments of the RV X representing the i.i.d. ambient data sequence $x(n)$ are finite. These conditions on the moments of $x(n)$ might be stronger than necessary but are nevertheless

reasonable and assumed here to simplify the derivation. One of the second order moments of the ambient sequence $x(n)$ is the sample energy which is given by:

$$\bar{E} = \mathbb{E} [|X|^2] = \frac{1}{N} \sum_{n=1}^N |x(n)|^2. \quad (9)$$

The result capturing the growth rate of S_N is provided in the following Lemma. Note that one has to be careful in deriving these concentration results since the sum sequence S_N is not composed of i.i.d elements. Please see the proof of the following Lemma for more details.

Lemma 1. *The expectation and variance of the sum sequence S_N both grow asymptotically of the order of N , i.e., $\mathbb{E}[S_N] = \Theta(N)$ and $\text{Var}[S_N] = \Theta(N)$, where $f(x) = \Theta(g(x))$ means that $f(x)$ is asymptotically bounded both from above and below by $g(x)$. As a consequence, the sequence M_N concentrates around $\mathbb{E}[M_N]$ when $N \rightarrow \infty$, where*

$$\mathbb{E}[M_N] = \mathbb{E}[|X|^2] + \frac{2\rho}{1-\rho} \left(1 - \frac{1-\rho^N}{N(1-\rho)}\right) |\mathbb{E}[X]|^2. \quad (10)$$

Proof: See Appendix A. ■

B. Conditional Distributions of the Signal in \mathcal{M}_1

We derive the conditional distributions of the mean received signal Y for a general value of correlation factor ρ . From that, the special case of independent fading ($\rho = 0$) is given as a corollary. For scheme \mathcal{M}_1 , the null hypothesis \mathcal{H}_0 and the alternate hypothesis \mathcal{H}_1 correspond to the scenarios with backscatter data $b \equiv 0$ and $b \equiv 1$ (which also correspond to the transmitted message bit $m \equiv 0$ and $m \equiv 1$ in this case), respectively.

1) *Null Hypothesis \mathcal{H}_0 :* In the AR model considered in this paper for the time-selective fading, the channel gain evolves with time according to (4), which can be described as a weighted average of the previous channel gain and a new variable. Due to this dependence of the current channel gain on the previous gains, the received signal samples are correlated, and hence the co-variances of the samples are non-zero in general. As a consequence, both the variances and co-variances of the signal samples have to be evaluated to derive the variance of the mean received signal Y . We transform the expression for each received signal sample into a sum representation of independent RVs. This will simplify the evaluation of both the variance of each signal sample and

the subsequent evaluation of the variance of the mean received signal. This can be represented in the following way:

$$y(n) = h_r(n)x(n) + w(n) = \left(\rho^{n-1}h_r(1) + \sqrt{1-\rho^2} \left\{ \sum_{k=1}^{n-1} \rho^{n-k-1} g_r(k) \right\} \right) x(n) + w(n), \quad (11)$$

where the channel gain $h_r(1)$ in the first time slot of a window can be independently configured.

Lemma 2. *The probability density function (PDF) of Y conditioned on \mathcal{H}_0 for the scheme \mathcal{M}_1 is characterized by the complex Gaussian distribution whose parameters are given by:*

$$\mathcal{H}_0 : Y_{\mathcal{M}_1} \sim \mathcal{CN} (0, \text{Var}_0^{\text{SA}}), \quad (12)$$

where $\text{Var}_0^{\text{SA}} = \frac{\sigma_h^2 \mathbb{E}[|X|^2] + \sigma_h^2 \frac{2\rho}{1-\rho} \left(1 - \frac{1-\rho^N}{N(1-\rho)} \right) |\mathbb{E}[X]|^2 + \sigma_n^2}{N}$ is the conditional variance of \mathcal{H}_0 .

Proof: See Appendix B. ■

The result is true for all $\rho \in [0, 1)$ and the special case of independent fading analyzed in the conference version of this paper [1] can be obtained by configuring ρ to 0. This is presented in the following Corollary.

Corollary 1. *The PDF of Y conditioned on \mathcal{H}_0 for an independent fading process under the scheme \mathcal{M}_1 is given by:*

$$\mathcal{H}_0 : Y_{\mathcal{M}_1} \sim \mathcal{CN} \left(0, \frac{\bar{E}\sigma_h^2 + \sigma_n^2}{N} \right). \quad (13)$$

Proof: Substituting $\rho = 0$ and $\bar{E} = \mathbb{E}[|X|^2]$ in (12) will give the result. ■

2) *Alternate Hypothesis \mathcal{H}_1 :* The received signal for a sample n , where $1 \leq n \leq N$ under the alternate hypothesis \mathcal{H}_1 is given by:

$$y(n) = h_r(n)x(n) + \underbrace{\alpha h_b(n)h_t(n)x(n)}_{y_b(n)} + w(n), \quad (14)$$

where $h_r(n)$, $h_b(n)$ and $h_t(n)$ are the fading gains following the process defined by (5). Unlike the case of \mathcal{H}_0 , further work is needed to derive the distribution for \mathcal{H}_1 since the conditional distribution of each sample is not complex Gaussian anymore. However, we preserve the Gaussian property of the samples by further conditioning on $h_b(n)$ and show that this conditional distribution asymptotically matches the true distribution. Only the distribution corresponding to $y_b(n)$ is needed to be derived and the sequence $M_N^b = \sum_{n_1, n_2} \rho^{|n_1 - n_2|} h_b(n_1)h_b^*(n_2)x(n_1)x^*(n_2)$

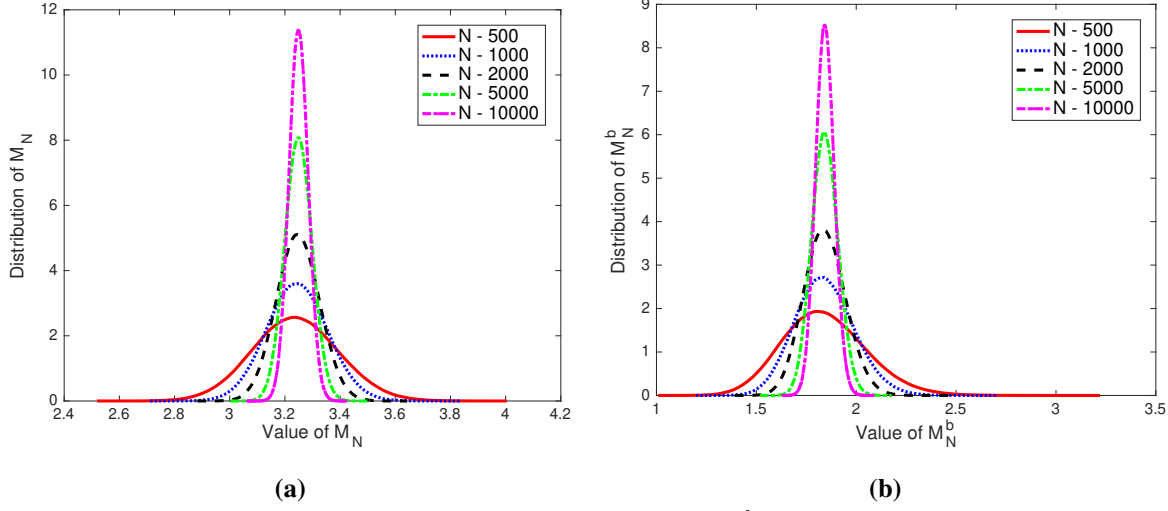


Fig. 3: Probability density functions of (a) M_N and (b) M_N^b for varying N with $\rho = 0.6$.

related to $y_b(n)$ is the corresponding parameter of \mathcal{H}_1 , similar to M_N of \mathcal{H}_0 . The following Lemma captures this analysis on the conditional distribution of \mathcal{H}_1 .

Lemma 3. *The PDFs of Y conditioned on \mathcal{H}_1 for the scheme \mathcal{M}_1 is characterized by the complex Gaussian distribution whose parameters are given by:*

$$\mathcal{H}_1 : Y_{\mathcal{M}_1} \sim \mathcal{CN} (0, \text{Var}_1^{\text{SA}}), \quad (15)$$

where $\text{Var}_1^{\text{SA}} = \frac{\sigma_h^2 (1 + |\alpha|^2 \sigma_h^2) \mathbb{E}[|X|^2] + \sigma_h^2 \left[\frac{2\rho}{1-\rho} \left(1 - \frac{1-\rho^N}{N(1-\rho)} \right) + |\alpha|^2 \sigma_h^2 \frac{2\rho^2}{1-\rho^2} \left(1 - \frac{1-\rho^{2N}}{N(1-\rho^2)} \right) \right] \mathbb{E}[|X|^2] + \sigma_n^2}{N}$ is the conditional variance of \mathcal{H}_1 .

Proof: See Appendix C. ■

Corollary 2. *The PDF of Y conditioned on \mathcal{H}_1 for an independent fading process under the scheme \mathcal{M}_1 is given by:*

$$\mathcal{H}_1 : Y_{\mathcal{M}_1} \sim \mathcal{CN} \left(0, \frac{\bar{E} \sigma_h^2 (1 + |\alpha|^2 \sigma_h^2) + \sigma_n^2}{N} \right). \quad (16)$$

Proof: Substituting $\rho = 0$ and $\bar{E} = \mathbb{E}[|X|^2]$ in (15) will give the result. ■

The analysis related to Lemma 1 on the asymptotic growth rate of S_N and the conditional distributions corresponding to the two hypotheses in Lemmas 2 and 3 are discussed now by comparing the simulation and theoretical results. The plots for the distributions of M_N and M_N^b with increasing sample size N are shown in Figs. 3a and 3b, where it can be observed that the mean values remain constant while their variances decrease as the signal sample size increases.

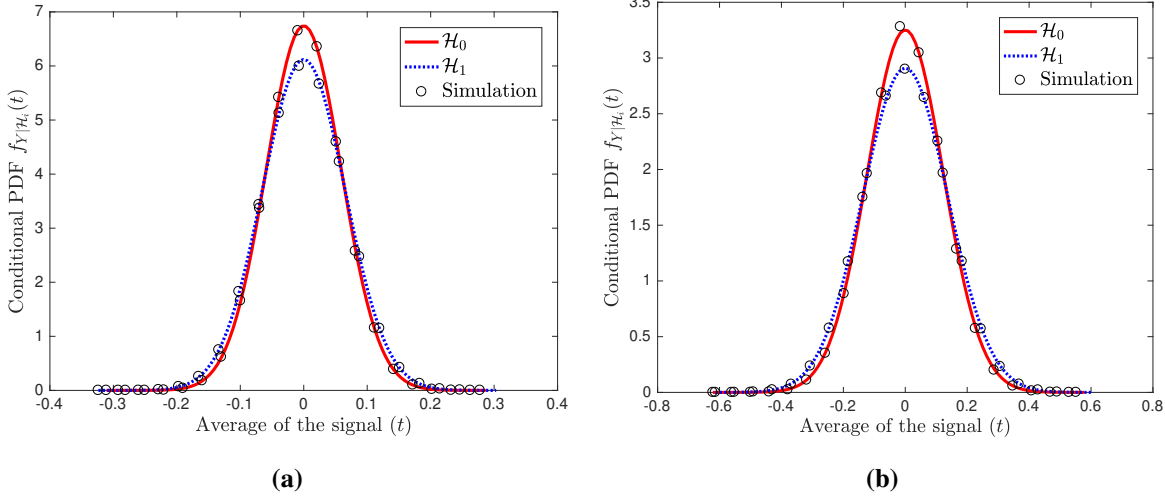


Fig. 4: Conditional density functions of \mathcal{H}_0 and \mathcal{H}_1 : (a) $\rho = 0.5$, $N=500$, (b) $\rho = 0.99$, $N=5000$.

The conditional distributions corresponding to the two hypotheses are compared in Figs. 4a and 4b. As one increases the correlation factor ρ , the sample-size N of the averaging operation required for the convergence of the simulation and theoretical results also increases.

C. Conditional Distributions of the Signal in \mathcal{M}_2

For scheme \mathcal{M}_2 , the two hypotheses are re-defined based on the actual message data m . The null hypothesis \mathcal{H}_0 corresponds to the scenario $m \equiv 0$ while the alternate hypothesis \mathcal{H}_1 corresponds to the case of $m \equiv 1$. To transmit the message bits $m \equiv 0$ and $m \equiv 1$, the transmitter will send codewords $[0\ 1]$ or $[1\ 0]$, respectively. Therefore, we need to derive the joint conditional distributions of the received signal over the two symbols for scheme \mathcal{M}_2 .

Lemma 4. *The joint PDFs of $Y_{\mathcal{M}_2}[0]$ and $Y_{\mathcal{M}_2}[1]$ conditioned on \mathcal{H}_0 and \mathcal{H}_1 for the scheme \mathcal{M}_2 are respectively given by:*

$$\mathcal{H}_0 : f_{Y_{\mathcal{M}_2}[0], Y_{\mathcal{M}_2}[1]}(y_0, y_1) = \frac{e^{-\left(\frac{|y_0|^2}{\text{Var}_0^{\text{SA}}} + \frac{|y_1|^2}{\text{Var}_1^{\text{SA}}}\right)}}{\pi \sqrt{\text{Var}_0^{\text{SA}} \text{Var}_1^{\text{SA}}}}, \quad (17)$$

$$\mathcal{H}_1 : f_{Y_{\mathcal{M}_2}[0], Y_{\mathcal{M}_2}[1]}(y_0, y_1) = \frac{e^{-\left(\frac{|y_0|^2}{\text{Var}_1^{\text{SA}}} + \frac{|y_1|^2}{\text{Var}_0^{\text{SA}}}\right)}}{\pi \sqrt{\text{Var}_0^{\text{SA}} \text{Var}_1^{\text{SA}}}}, \quad (18)$$

where Var_0^{SA} and Var_1^{SA} are defined earlier while deriving the conditional distributions of \mathcal{M}_1 .

Proof: See Appendix D. ■

Corollary 3. The joint PDFs of $Y_{\mathcal{M}_2}[0]$ and $Y_{\mathcal{M}_2}[1]$ conditioned on \mathcal{H}_0 and \mathcal{H}_1 for the scheme \mathcal{M}_2 in an independent fading process are respectively given by:

$$\mathcal{H}_0 : f_{Y_{\mathcal{M}_2}[0], Y_{\mathcal{M}_2}[1]}(y_0, y_1) = \frac{\exp \left\{ - \left(\frac{|y_0|^2}{\frac{\bar{E}\sigma_h^2 + \sigma_n^2}{N}} + \frac{|y_1|^2}{\frac{\bar{E}\sigma_h^2(1+|\alpha|^2\sigma_h^2) + \sigma_n^2}{N}} \right) \right\}}{\frac{\pi}{N} \sqrt{(\bar{E}\sigma_h^2 + \sigma_n^2)(\bar{E}\sigma_h^2(1+|\alpha|^2\sigma_h^2) + \sigma_n^2)}}, \quad (19)$$

$$\mathcal{H}_1 : f_{Y_{\mathcal{M}_2}[0], Y_{\mathcal{M}_2}[1]}(y_0, y_1) = \frac{\exp \left\{ - \left(\frac{|y_0|^2}{\frac{\bar{E}\sigma_h^2(1+|\alpha|^2\sigma_h^2) + \sigma_n^2}{N}} + \frac{|y_1|^2}{\frac{\bar{E}\sigma_h^2 + \sigma_n^2}{N}} \right) \right\}}{\frac{\pi}{N} \sqrt{(\bar{E}\sigma_h^2 + \sigma_n^2)(\bar{E}\sigma_h^2(1+|\alpha|^2\sigma_h^2) + \sigma_n^2)}}. \quad (20)$$

Proof: Substituting $\rho = 0$ and $\bar{E} = \mathbb{E}[|X|^2]$ in (17) and (18) will give the results. \blacksquare

D. Bit Error Rate

From the analysis of conditional distributions, we see that the PDFs under the two hypotheses have the same mean but different variances. For the scheme \mathcal{M}_1 , the complex Gaussian PDFs of the two hypotheses derived above are directly compared to obtain the optimal detection threshold, while for the scheme \mathcal{M}_2 , the joint distribution of the mean received signals corresponding to the two symbol durations of the backscatter data are compared to derive the optimal threshold.

Theorem 1. The average BER of scheme \mathcal{M}_1 for a single antenna receiver is given by:

$$P_{\mathcal{M}_1}^{SA}(e) = \frac{1}{2} - \frac{1}{2} e^{-\frac{T_{\mathcal{M}_1}^{SA}}{\text{Var}_1^{SA}}} + \frac{1}{2} e^{-\frac{T_{\mathcal{M}_1}^{SA}}{\text{Var}_0^{SA}}}, \quad (21)$$

where $T_{\mathcal{M}_1}^{SA} = \ln \left(\frac{\text{Var}_1^{SA}}{\text{Var}_0^{SA}} \right) \frac{\text{Var}_1^{SA} \text{Var}_0^{SA}}{\text{Var}_1^{SA} - \text{Var}_0^{SA}}$ is the optimal detection threshold of scheme \mathcal{M}_1 .

Proof: See Appendix E. \blacksquare

Theorem 2. The average BER of scheme \mathcal{M}_2 for a single antenna receiver is given by:

$$P_{\mathcal{M}_2}^{SA}(e) = \left(1 + \frac{\text{Var}_1^{SA}}{\text{Var}_0^{SA}} \right)^{-1}. \quad (22)$$

Proof: See Appendix F. \blacksquare

Asymptotic analysis: The ratio of the variances corresponding to the null and alternate hypotheses of a single antenna receiver that appears in (22) is given by:

$$K = \frac{\text{Var}_1^{SA}}{\text{Var}_0^{SA}} = 1 + \frac{|\alpha|^2 \sigma_h^4 \left\{ \mathbb{E}[|X|^2] + \frac{2\rho^2}{1-\rho^2} \left(1 - \frac{1-\rho^{2N}}{N(1-\rho^2)} \right) |\mathbb{E}[X]|^2 \right\}}{\sigma_h^2 \left\{ \mathbb{E}[|X|^2] + \frac{2\rho}{1-\rho} \left(1 - \frac{1-\rho^N}{N(1-\rho)} \right) |\mathbb{E}[X]|^2 \right\} + \sigma_n^2}$$

$$= 1 + \frac{|\alpha|^2 \sigma_h^4 \left\{ 1 + \frac{2\rho^2}{1-\rho^2} \left(1 - \frac{1-\rho^{2N}}{N(1-\rho^2)} \right) \frac{|\mathbb{E}[X]|^2}{\mathbb{E}[|X|^2]} \right\}}{\sigma_h^2 \left\{ 1 + \frac{2\rho}{1-\rho} \left(1 - \frac{1-\rho^N}{N(1-\rho)} \right) \frac{|\mathbb{E}[X]|^2}{\mathbb{E}[|X|^2]} \right\} + \text{SNR}^{-1}} \quad (23)$$

The asymptotic conditional BER of the first encoding scheme \mathcal{M}_1 can be derived as:

$$\begin{aligned} P_{\mathcal{M}_1}^{\text{SA}}(e_{\text{asym}}) &= \lim_{\text{SNR} \rightarrow \infty} \frac{1}{2} \left(1 - e^{-\frac{T_{\mathcal{M}_1}^{\text{SA}}}{\text{Var}_1^{\text{SA}}}} + e^{-\frac{T_{\mathcal{M}_1}^{\text{SA}}}{\text{Var}_0^{\text{SA}}}} \right) \\ &\stackrel{(a)}{=} \lim_{\text{SNR} \rightarrow \infty} \frac{1}{2} \left(1 - K^{\frac{-1}{K-1}} + \frac{1}{K}^{\frac{1}{1-K}} \right) \stackrel{(b)}{=} \frac{1}{2} \left(1 - K_{\infty}^{\frac{-1}{K_{\infty}-1}} + \frac{1}{K_{\infty}}^{\frac{1}{1-K_{\infty}}} \right), \end{aligned} \quad (24)$$

where (a) results from the substitution of the expression for $T_{\mathcal{M}_1}^{\text{SA}}$ and replacing the ratio $\frac{\text{Var}_1^{\text{SA}}}{\text{Var}_0^{\text{SA}}}$ with K defined earlier, and (b) follows from the substitution of K with K_{∞} obtained as $\text{SNR} \rightarrow \infty$.

Similarly, the asymptotic BER of the second encoding scheme \mathcal{M}_2 can be derived as follows:

$$\begin{aligned} P_{\mathcal{M}_2}^{\text{SA}}(e_{\text{asym}}) &= \lim_{\text{SNR} \rightarrow \infty} \left(2 + \frac{|\alpha|^2 \sigma_h^4 + |\alpha|^2 \sigma_h^4 \frac{2\rho^2}{1-\rho^2} \left(1 - \frac{1-\rho^{2N}}{N(1-\rho^2)} \right) |\mathbb{E}[X]|^2 \{ \mathbb{E}[|X|^2] \}^{-1}}{\sigma_h^2 + \sigma_h^2 \frac{2\rho}{1-\rho} \left(1 - \frac{1-\rho^N}{N(1-\rho)} \right) |\mathbb{E}[X]|^2 \{ \mathbb{E}[|X|^2] \}^{-1} + \text{SNR}^{-1}} \right)^{-1} \\ &= \left(2 + \frac{|\alpha|^2 \sigma_h^2 + |\alpha|^2 \sigma_h^2 \frac{2\rho^2}{1-\rho^2} \left(1 - \frac{1-\rho^{2N}}{N(1-\rho^2)} \right) |\mathbb{E}[X]|^2 \{ \mathbb{E}[|X|^2] \}^{-1}}{1 + \frac{2\rho}{1-\rho} \left(1 - \frac{1-\rho^N}{N(1-\rho)} \right) |\mathbb{E}[X]|^2 \{ \mathbb{E}[|X|^2] \}^{-1}} \right)^{-1}. \end{aligned} \quad (25)$$

Remark 3. Clearly, the BER expressions of the two encoding schemes \mathcal{M}_1 and \mathcal{M}_2 for a single antenna receiver are independent of N under certain conditions such as $\rho = 0$ or/and $\mathbb{E}[X] = 0$. Furthermore, the asymptotic BER values, with respect to the increasing SNR, reach an error floor instead of converging to zero. This error floor corresponding to the two schemes is numerically demonstrated later in Fig. 5a. This necessitates the need to develop better techniques to decode data in a time-selective channel, which takes us to the next main contribution of this paper.

IV. DETECTION AT A MULTI-ANTENNA RECEIVER

The main reason for the poor BER performance of single antenna receiver is the presence of the direct path from ambient source which only acts as interference since it does not carry any backscatter data. For a multi-antenna receiver, the signal impinging on neighboring antenna element is a phase shifted version of the signal on the first antenna (along with independent additive noise). The received signal at this receiver is already given in (8). Observe that the phase offset of the backscatter link is independent of the phase offset of the direct link. We can remove the direct link component by inverting the phase offset of the direct link at the second antenna and subtracting it from the signal at the first antenna.

A. Conditional Distributions of the Signal

After multiplying the signal at second antenna element by the phase-offset inversion component $e^{-j\phi_1}$ and subtracting from the signal at the first antenna, we have the following effective signal:

$$\mathcal{H}_0 : y_{\text{eff}}(n) = e^{-j\phi_1} y_1(n) - y_0(n) = \tilde{w}_1(n) - w_0(n), \quad (26)$$

$$\mathcal{H}_1 : y_{\text{eff}}(n) = e^{-j\phi_1} y_1(n) - y_0(n) = \alpha(e^{j(\phi_2-\phi_1)} - 1) h_t(n) h_b(n) x(n) + \tilde{w}_1(n) - w_0(n). \quad (27)$$

The average of the effective signal samples $y_{\text{eff}}(n)$ given by $Y = \frac{1}{N} \sum_{n=1}^N y_{\text{eff}}(n)$ is used to decode the transmitted data at the multi-antenna receiver.

Lemma 5. *The PDFs of Y conditioned on the hypothesis \mathcal{H}_i are given by:*

$$\mathcal{H}_i : Y \sim \mathcal{CN}(0, \text{Var}_i^{\text{MA}}), \quad (28)$$

where $\text{Var}_0^{\text{MA}} = \frac{2\sigma_n^2}{N}$ and $\text{Var}_1^{\text{MA}} = \frac{4 \sin^2\left(\frac{\phi_2-\phi_1}{2}\right) |\alpha|^2 \sigma_h^4 \left\{ \mathbb{E}[|X|^2] + \frac{2\rho^2}{1-\rho^2} \left(1 - \frac{1-\rho^{2N}}{N(1-\rho^2)}\right) |\mathbb{E}[X]|^2 \right\} + 2\sigma_n^2}{N}$ are the conditional variances under hypotheses \mathcal{H}_0 and \mathcal{H}_1 , respectively.

Proof: See Appendix G. ■

While there are multiple ways of estimating the phase-offset inversion component $e^{-j\phi_1}$ of the direct link, we have provided one in Appendix I.

B. Bit Error Rate

Theorem 3. *The average BER of the encoding schemes \mathcal{M}_1 and \mathcal{M}_2 in a multi-antenna receiver are respectively given by:*

$$P_{\mathcal{M}_1}^{\text{MA}}(e) = \int_{-\pi}^{\pi} \int_{-\pi}^{\pi} \frac{1}{2\pi} \times \frac{1}{2\pi} \times \frac{1}{2} \left(1 - e^{-\frac{T_{\mathcal{M}_1}^{\text{MA}}}{\text{Var}_1^{\text{MA}}}} + e^{-\frac{T_{\mathcal{M}_1}^{\text{MA}}}{\text{Var}_0^{\text{MA}}}} \right) d\theta_1 d\theta_2, \quad (29)$$

$$P_{\mathcal{M}_2}^{\text{MA}}(e) = \int_{-\pi}^{\pi} \int_{-\pi}^{\pi} \frac{1}{2\pi} \times \frac{1}{2\pi} \times \frac{1}{2} \times \frac{\sigma_n^2}{\sin^2\left\{\frac{\pi}{\lambda}d(\cos\theta_2 - \cos\theta_1)\right\} |\alpha|^2 \sigma_h^4 \left\{ \mathbb{E}[|X|^2] + \frac{2\rho^2}{1-\rho^2} \left(1 - \frac{1-\rho^{2N}}{N(1-\rho^2)}\right) |\mathbb{E}[X]|^2 \right\} + \sigma_n^2} d\theta_1 d\theta_2, \quad (30)$$

where $T_{\mathcal{M}_1}^{\text{MA}} = \ln\left(\frac{\text{Var}_1^{\text{MA}}}{\text{Var}_0^{\text{MA}}}\right) \frac{\text{Var}_1^{\text{MA}} \text{Var}_0^{\text{MA}}}{\text{Var}_1^{\text{MA}} - \text{Var}_0^{\text{MA}}}$ is the optimal detection threshold of scheme \mathcal{M}_1 .

Proof: See Appendix H. ■

Asymptotic analysis: The ratio of the variances corresponding to the null and alternate hypotheses of a multi-antenna receiver that appears in (30) is given by:

$$K = \frac{\text{Var}_1^{\text{MA}}}{\text{Var}_0^{\text{MA}}} = \frac{4 \sin^2 \left(\frac{\phi_2 - \phi_1}{2} \right) |\alpha|^2 \sigma_h^4 \left\{ \mathbb{E}[|X|^2] + \frac{2\rho^2}{1-\rho^2} \left(1 - \frac{1-\rho^{2N}}{N(1-\rho^2)} \right) |\mathbb{E}[X]|^2 \right\} + 2\sigma_n^2}{2\sigma_n^2} \\ = 1 + 2 \sin^2 \left(\frac{\phi_2 - \phi_1}{2} \right) |\alpha|^2 \sigma_h^4 \left\{ 1 + \frac{2\rho^2}{1-\rho^2} \left(1 - \frac{1-\rho^{2N}}{N(1-\rho^2)} \right) \frac{|\mathbb{E}[X]|^2}{\mathbb{E}[|X|^2]} \right\} + \text{SNR} \quad (31)$$

The asymptotic conditional BER of the first encoding scheme \mathcal{M}_1 can be derived as:

$$P_{\mathcal{M}_1}^{\text{MA}}(e_{\text{asym}} | \phi_1, \phi_2) = \frac{1}{2} \left(1 - e^{-\frac{T_{\mathcal{M}_1}^{\text{MA}}}{\text{Var}_1^{\text{MA}}}} + e^{-\frac{T_{\mathcal{M}_1}^{\text{MA}}}{\text{Var}_0^{\text{MA}}}} \right) \stackrel{(a)}{=} \frac{1}{2} \left(1 - K^{\frac{-1}{K-1}} + \frac{1}{K}^{\frac{1}{1-K}} \right) \stackrel{(b)}{=} 0 \quad (32)$$

where (a) results from substituting the expression for $T_{\mathcal{M}_1}^{\text{MA}}$ and replacing the ratio $\frac{\text{Var}_1^{\text{MA}}}{\text{Var}_0^{\text{MA}}}$ with K defined earlier, and (b) follows from the standard limit result $\lim_{x \rightarrow \infty} (x)^{-1/x-1} = 1$, and $\frac{1}{K} \rightarrow 0$ as $\text{SNR} \rightarrow \infty$. Similarly, the asymptotic conditional BER of the scheme \mathcal{M}_2 can be derived as:

$$P_{\mathcal{M}_2}^{\text{MA}}(e_{\text{asym}} | \phi_1, \phi_2) \\ = \lim_{\text{SNR} \rightarrow \infty} \frac{\text{SNR}^{-1}}{2 \left(\sin^2 \left(\frac{\phi_2 - \phi_1}{2} \right) |\alpha|^2 \sigma_h^4 \left\{ 1 + \frac{2\rho^2}{1-\rho^2} \left(1 - \frac{1-\rho^{2N}}{N(1-\rho^2)} \right) \frac{|\mathbb{E}[X]|^2}{\mathbb{E}[|X|^2]} \right\} + \text{SNR}^{-1} \right)} = 0. \quad (33)$$

Remark 4. *In case of fast-fading ($\rho = 0$), where the fading gains are independent across different ambient symbols, the average BER is only dependent on the expected value of the energy of the ambient symbol. This special case concurs with our analysis in [1]. Alternatively, if the mean value of the ambient symbol is zero (which is the case for most of the modulation schemes in digital communication), then again the average BER is only dependent on the expected value of the energy. Finally, it can be inferred from the expression that the average BER is an increasing function of the correlation factor ρ .*

V. NUMERICAL RESULTS AND DISCUSSION

In this section, we verify the accuracy of analytic results derived in the previous sections by comparing them with Monte-Carlo simulations and also provide some useful system design insights. The reflection coefficient Γ_1 is configured appropriately to set the parameter α that will result in signal attenuation of 1.1 dB as mentioned in [3]. The variance σ_h^2 of the fading gain of each communication link is set to 1. The BER performance of the two receivers for the two encoding schemes \mathcal{M}_1 and \mathcal{M}_2 , related to the cases of independent fading ($\rho = 0$) and/or ambient sequence with zero expectation ($\mathbb{E}[X] = 0$), are compared in Fig. 5a. We

observe that with increasing SNR, the BER saturates very quickly for a single antenna receiver and does not improve any further. Even changing the encoding scheme from \mathcal{M}_1 to \mathcal{M}_2 does not offer any noticeable improvement. This behavior can be attributed to the dependence of a non-coherent detector on differences in the conditional variances of the received symbol. With the strong interference from power source, the variances of the two hypotheses scale similarly with increasing SNR. On the other hand, as shown in Fig. 5a, the multi-antenna receiver can drastically improve the BER of \mathcal{M}_1 by removing the direct path from the ambient power source. In this case, BER decreases continuously without reaching any error floor. Additionally, by using scheme \mathcal{M}_2 , the multi-antenna receiver can obtain an additional gain of atleast 3 dB as shown in Fig. 5a. When the interference from the direct link is removed in the multi-antenna receiver, only variance of the alternate hypothesis scales proportionally to the increasing SNR that ultimately results in the improved BER. Further, as shown in Fig. 5b, the average BER is independent of the signal sample size N under these two cases.

The results for more general cases of time-correlated fading and the ambient sequence with non-zero expectation are discussed now. The error floor for the two encoding schemes in a single antenna receiver decreases with correlation factor ρ , as shown in Figs. 6a and 6b. It can be verified from these figures that the numerically obtained BER floor values of the single antenna receiver match with the asymptotic BER analytically derived in (24) and (25). The BER performance of \mathcal{M}_1 with increasing SNR in a multi-antenna receiver for different values of the correlation factor ρ is presented in Fig. 7a, where it can be seen that the BER improves with increasing ρ . Likewise, the BER performance with increasing sample size N for varying ρ is shown in Fig. 7b, and interestingly, the BER increases and saturates quickly with increasing N . However, as expected, there is an increasing mismatch between the simulated and theoretical results of BER at lower values of N as the value of ρ is increased. This mismatch occurs due to the need of a larger sample-size N for the averaging operation, so that the simulation and theoretical results converge with increasing ρ . Similar comparisons of the BER performance of \mathcal{M}_2 with increasing SNR and N for varying ρ are shown in Figs. 8a and 8b, respectively. The waterfall curves for the two encoding schemes with increasing SNR, as shown in Figs. 7a and 8a, also validate our asymptotic BER analysis presented in (32) and (33) for the multi-antenna receiver. The BER improvement observed with increasing ρ and N can be attributed to the increment in variance of the alternate hypothesis while the variance of the null hypothesis remains the same.

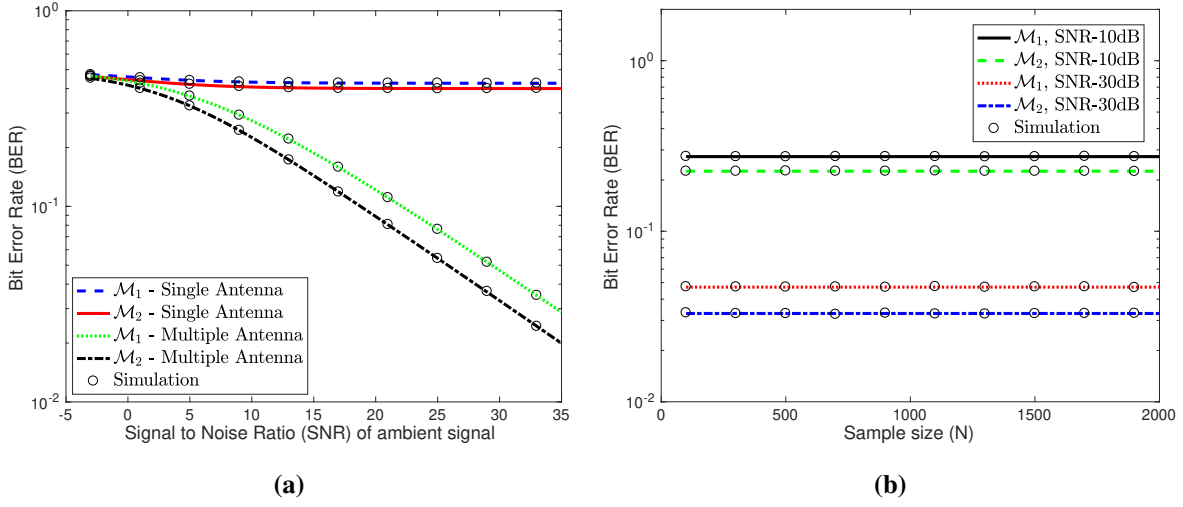


Fig. 5: BER performance of the two encoding schemes for the single and multiple antenna receivers under independent fading and/or ambient sequence with $\mathbb{E}[X] = 0$.

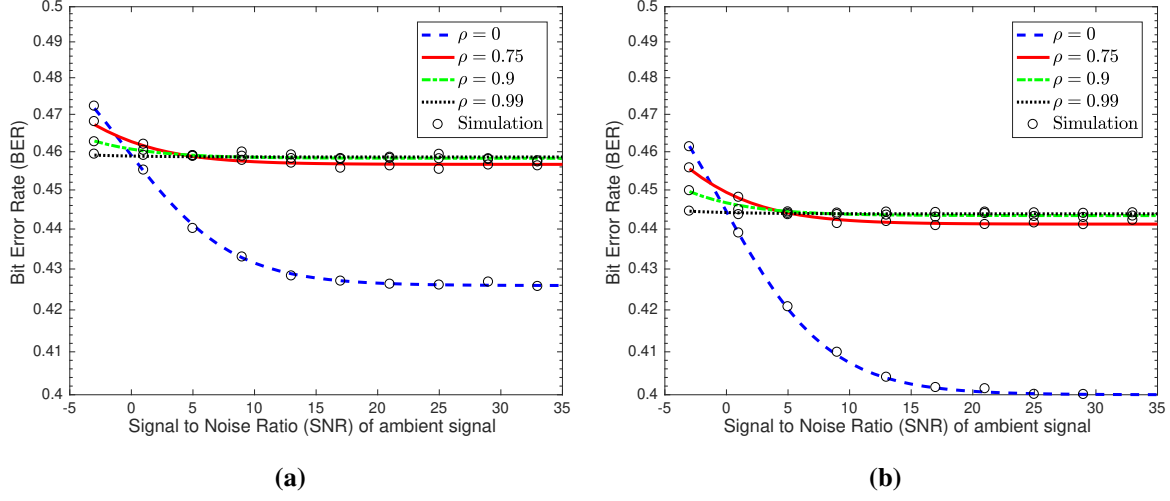


Fig. 6: BER performance and error floor of single antenna receiver under encoding schemes (a) \mathcal{M}_1 and (b) \mathcal{M}_2 .

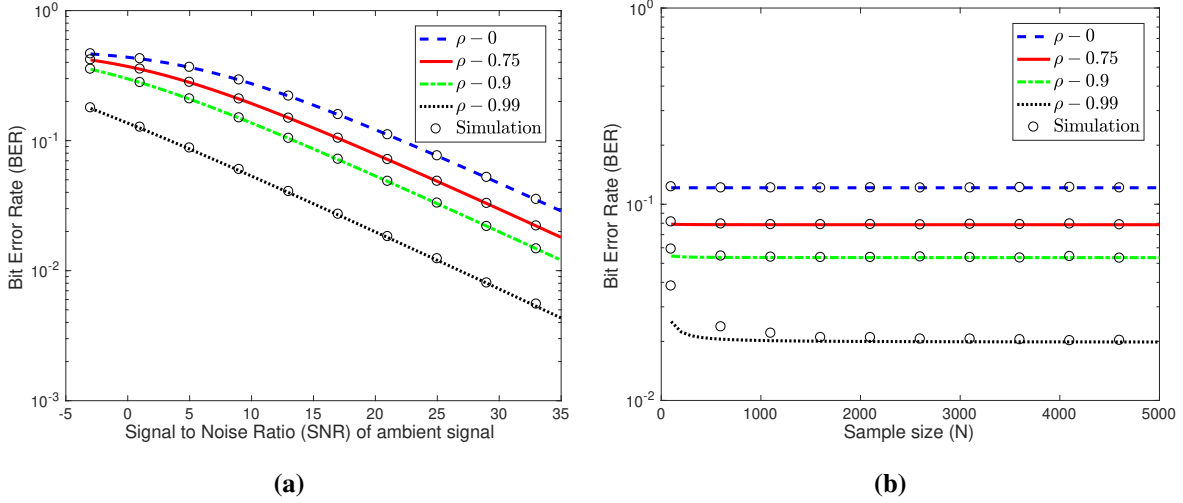


Fig. 7: (a) BER vs SNR comparison for varying correlation factor ρ in encoding scheme \mathcal{M}_1 and $N = 5000$, (b) BER vs N comparison for varying correlation factor ρ in encoding scheme \mathcal{M}_1 and SNR = 20 dB.

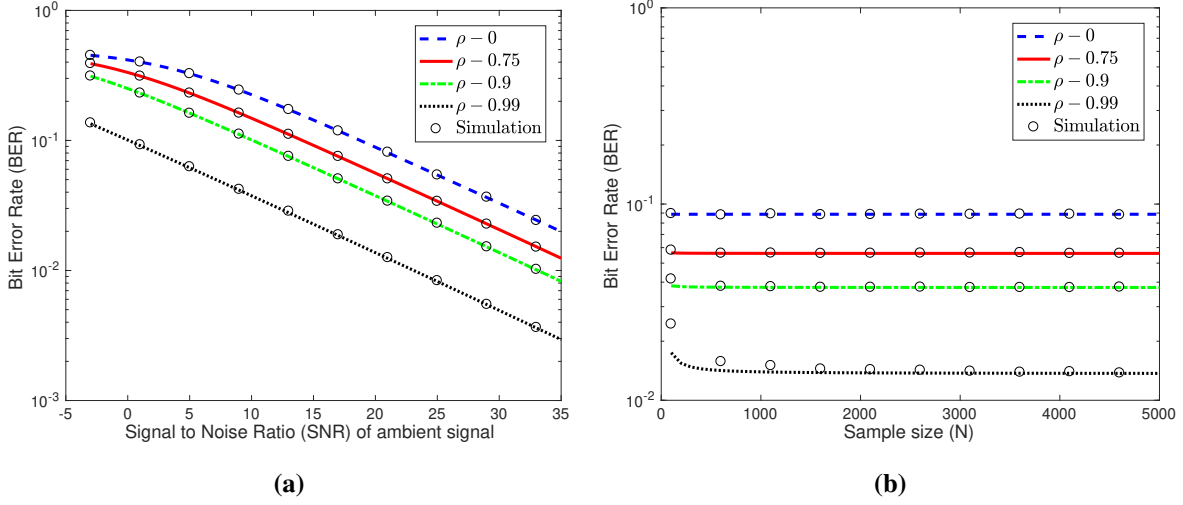


Fig. 8: (a) BER vs SNR comparison for varying correlation factor ρ in encoding scheme \mathcal{M}_2 and $N = 5000$, (b) BER vs N comparison for varying correlation factor ρ in encoding scheme \mathcal{M}_2 and SNR = 20 dB.

VI. CONCLUSION

Ambient backscatter systems have mainly been studied for low mobility scenarios that are modeled using a block fading channel. While the block fading model is sufficient for stationary environments like home and office, a time-selective fading channel is more suitable for non-stationary environments, such as roads and campuses. Therefore, in this paper, we have investigated the performance of an ambient backscatter system by studying the design, encoding schemes and BER of a non-coherent detector under time-selective fading channels. To the best of our knowledge, this is the first work that has incorporated both non-coherent detection and time-selective fading channel into the ambient backscatter setup. Unlike the conventional architecture used in the literature, which is implemented using the average of the energy of the received signal samples, a new receiver architecture based on the direct average of the received signal samples is proposed. The new architecture is simpler to implement and also lends tractability to the asymptotic analysis, which is useful for the derivation of optimal detection strategies. In the analysis, we have shown that a BER floor exists for a single antenna receiver due to the interference created by the direct link from the ambient source, thereby resulting in an unacceptable performance. The BER performance is drastically improved using a multi-antenna receiver by tracking the AoA of the direct link and use it to eliminate the interference. For a general case of the time-selective fading, the BER improves with increasing signal sample size but saturates to an asymptotic BER. Additionally, the BER is observed to improve with increasing temporal-correlation of the time-selective fading channel. A natural extension of this

work is to implement an ambient backscatter system that can function in a channel with multiple angular paths at the receiver.

APPENDIX

A. Proof of Lemma 1

The value of the summation $\sum_{n_1 \neq n_2} \rho^{|n_1 - n_2|}$, which is used in the subsequent steps is given by:

$$\sum_{n_1 \neq n_2} \rho^{|n_1 - n_2|} = \frac{2\rho}{1 - \rho} \left(N - \frac{1 - \rho^N}{1 - \rho} \right), \quad 0 \leq \rho < 1. \quad (34)$$

The expectation of the sum sequence S_N can be evaluated easily as follows:

$$\begin{aligned} \mathbb{E}[S_N] &= \mathbb{E} \left[\sum_{n_1, n_2} \rho^{|n_1 - n_2|} x(n_1) x^*(n_2) \right] = \sum_n \mathbb{E}[|x(n)|^2] + \sum_{n_1 \neq n_2} \rho^{|n_1 - n_2|} \mathbb{E}[x(n_1)] \mathbb{E}[x^*(n_2)] \\ &\stackrel{(a)}{=} \sum_n \mathbb{E}[|X|^2] + \sum_{n_1 \neq n_2} \rho^{|n_1 - n_2|} |\mathbb{E}[X]|^2 \stackrel{(b)}{=} N \mathbb{E}[|X|^2] + \frac{2\rho}{1 - \rho} \left(N - \frac{1 - \rho^N}{1 - \rho} \right) |\mathbb{E}[X]|^2, \end{aligned} \quad (35)$$

where (a) and (b) follow from the assumption that the ambient sequence $x(n)$ is i.i.d., and the value of summation given in (34), respectively. It can be easily observed that the expectation of this sum grows asymptotically of the order of N , meaning $\mathbb{E}[S_N] = \Theta(N)$. Using this, the expectation of $M_N = \frac{S_N}{N}$ can be shown to be a constant, whose value is given in (10).

The variance of the sum sequence S_N can first be simplified as given below:

$$\begin{aligned} \text{Var}[S_N] &= \mathbb{E} \left[\left(\sum_{i_1, j_1} \rho^{|i_1 - j_1|} x(i_1) x^*(j_1) \right) \left(\sum_{i_2, j_2} \rho^{|i_2 - j_2|} x^*(i_2) x(j_2) \right) \right] - \mathbb{E}[S_N]^2 \\ &= \mathbb{E} \left[\sum_{i_1} \sum_{i_2} |x(i_1)|^2 |x(i_2)|^2 + 2 \sum_{i_1} \sum_{i_2 \neq j_2} \rho^{|i_2 - j_2|} |x(i_1)|^2 x^*(i_2) x(j_2) \right. \\ &\quad \left. + \sum_{i_1 \neq j_1} \sum_{i_2 \neq j_2} \rho^{|i_1 - j_1| + |i_2 - j_2|} x(i_1) x^*(j_1) x^*(i_2) x(j_2) \right] - \mathbb{E}[S_N]^2 \\ &\stackrel{(c)}{=} \sum_{i_1=i_2} \mathbb{E}[|X|^4] + \left\{ \sum_{i_1 \neq i_2} 1 + \sum_{i_1 \neq j_1} \rho^{2|i_1 - j_1|} - \left(\sum_i 1 \right)^2 \right\} \left(\mathbb{E}[|X|^2] \right)^2 \\ &\quad + 2 \sum_{i_1 \neq j_2} \rho^{|i_1 - j_2|} \mathbb{E}[X(X^*)^2] \mathbb{E}[X] + 2 \sum_{i_1 \neq i_2} \rho^{|i_1 - i_2|} \mathbb{E}[(X)^2 X^*] \mathbb{E}[X^*] + \sum_{i_1 \neq j_1} \rho^{2|i_1 - j_1|} |\mathbb{E}[X^2]|^2 \\ &\quad + 2 \left\{ \sum_{i_1 \neq i_2 \neq j_2} \rho^{|i_2 - j_2|} + \sum_{i_1 \neq j_1 \neq j_2} \rho^{|i_1 - j_1| + |i_1 - j_2|} - \sum_{i, i_1 \neq i_2} \rho^{|i_1 - i_2|} \right\} \mathbb{E}[|X|^2] |\mathbb{E}[X]|^2 \\ &\quad + \sum_{i_1 \neq i_2 \neq j_1} \rho^{|i_1 - j_1| + |i_2 - j_1|} \mathbb{E}[X^2] (\mathbb{E}[X^*])^2 + \sum_{i_1 \neq j_1 \neq j_2} \rho^{|i_1 - j_1| + |j_1 - j_2|} (\mathbb{E}[X^2])^* (\mathbb{E}[X])^2 \end{aligned}$$

$$+ \left\{ \sum_{i_1 \neq j_1 \neq i_2 \neq j_2} \rho^{|i_1-j_1|+|i_2-j_2|} - \left(\sum_{n_1 \neq n_2} \rho^{|n_1-n_2|} \right)^2 \right\} |\mathbb{E}[X]|^4, \quad (36)$$

where (c) follows from the piece-wise separation of different summations by permuting the indices i_1, i_2, j_1 and j_2 of the first term, and the expansion of the second term $\mathbb{E}[S_N]$.

Now, the main objective is to show that the variance, similar to the mean, also grows asymptotically of the order of N . The complete derivation of the expression for the variance is conceptually simple but tedious to present in a limited space. For this reason, we only provide a sketch of the proof, which is sufficient to understand the main methodology. Recall the assumption that the higher order moments of the sequence $x(n)$ upto the highest order present in (36) are finite. With this assumption, it is sufficient to prove that the coefficient of each moment increases of the order of N . The coefficient of $\mathbb{E}[|X|^4]$ is straightforward to obtain and is given by N . Using (34), it is again straightforward to show that $\sum_{i_1 \neq j_1} \rho^{2|i_1-j_1|}$ is a function N , and the summations $\sum_{i_1 \neq i_2} 1$ and $(\sum_i 1)^2$ are respectively given by N^2 and $N(N-1)$. Hence, the coefficient of $(\mathbb{E}[|X|^2])^2$ is proportional to N and increases asymptotically of the order of N . Then, the coefficients of $\mathbb{E}[X(X^*)^2] \mathbb{E}[X]$, $\mathbb{E}[(X)^2 X^*] \mathbb{E}[X^*]$ and $|\mathbb{E}[X^2]|^2$, given by either $\sum_{i_1 \neq j_1} \rho^{|i_1-j_1|}$ or $\sum_{i_1 \neq j_1} \rho^{2|i_1-j_1|}$, are already shown to be proportional to N . Similarly, the summation $\sum_{i_1 \neq j_1 \neq j_2} \rho^{|i_1-j_1|+|i_1-j_2|}$ can be evaluated by piece-wise categorization into different subsets and shown to grow of the order of N . In addition, the summations $\sum_{i_1 \neq i_2 \neq j_2} \rho^{|i_2-j_2|}$ and $\sum_{i_1 \neq i_2} \rho^{|i_1-i_2|}$ can both be shown to have the same factor for N^2 , and hence the coefficients of $|\mathbb{E}[X^2]|^2$, $\mathbb{E}[X^2] (\mathbb{E}[X^*])^2$ and $(\mathbb{E}[X^2])^* (\mathbb{E}[X])^2$ all increase at the order of N . Finally, it can also be shown that $\sum_{i_1 \neq j_1 \neq i_2 \neq j_2} \rho^{|i_1-j_1|+|i_2-j_2|}$ and $(\sum_{n_1 \neq n_2} \rho^{|n_1-n_2|})^2$ are both proportional to $N(N-1)$ with the same factor, which also means that $|\mathbb{E}[X]|^4$ grows of the order of N . Therefore, we can conclude that $\text{Var}[S_N]$ has a growth rate of N i.e., $\text{Var}[S_N] = \Theta(N)$. As a consequence, the variance of $M_N = \frac{S_N}{N}$ will be decreasing at the rate of $1/N$ asymptotically. This completes the proof.

B. Proof of Lemma 2

When conditioned on the signal $x(n)$, a sample of the received signal under \mathcal{H}_0 , as given in (11), is a complex Gaussian RV. As a result, the mean of these received samples can also be characterized as a complex Gaussian, *albeit* the samples are correlated with one another. Since the complex Gaussian RV is completely defined by its mean and variance, we are just required

to derive them. First, the conditional expectation and variance of an individual sample $y(n)$ can be derived respectively as:

$$\begin{aligned}\mathbb{E}[y(n)] &= \mathbb{E}\left[\left(\rho^{n-1}h_r(1) + \sqrt{1-\rho^2}\left\{\sum_{k=1}^{n-1}\rho^{n-k-1}g_r(k)\right\}\right)x(n) + w(n)\right] \\ &= \left(\rho^{n-1}\mathbb{E}[h_r(1)] + \sqrt{1-\rho^2}\left\{\sum_{k=1}^{n-1}\rho^{n-k-1}\mathbb{E}[g_r(k)]\right\}\right)x(n) + \mathbb{E}[w(n)] = 0, \\ \text{Var}[y(n)] &= \text{Var}\left[\rho^{n-1}h_r(1)x(n)\right] + \sum_{k=1}^{n-1}\text{Var}\left[\sqrt{1-\rho^2}\left\{\rho^{n-k-1}g_r(k)x(n)\right\}\right] + \text{Var}[w(n)] \\ &= \left(\rho^{2n-2} + \sum_{k=1}^{n-1}(1-\rho^2)\rho^{2n-2k-2}\right)\sigma_h^2|x(n)|^2 + \sigma_n^2 = \sigma_h^2|x(n)|^2 + \sigma_n^2.\end{aligned}$$

Similarly, the conditional covariance of any two distinct samples $y(i)$ and $y(j)$ is given by:

$$\begin{aligned}\text{Cov}[y(i), y(j)] &\stackrel{(a)}{=} \mathbb{E}[y(i)y^*(j)] \\ &= \mathbb{E}\left[\left(\rho^{i+j-2}|h_r[1]|^2 + \sqrt{1-\rho^2}\sum_{k_2=1}^{j-1}\rho^{i+j-k_2-2}h_r[1]g_r^*[k_2]\right)x(i)x^*(j) + \rho^{i-1}h_r[1]x(i)w^*(j)\right. \\ &\quad + \left(\sqrt{1-\rho^2}\sum_{k_1=1}^{i-1}\rho^{i+j-k_1-2}h_r^*[1]g_r[k_1] + (1-\rho^2)\sum_{k_1=1}^{i-1}\sum_{k_2=1}^{j-1}\rho^{i+j-k_1-k_2-2}g_r[k_1]g_r^*[k_2]\right)x(i)x^*(j) \\ &\quad + \sqrt{1-\rho^2}\sum_{k_1=1}^{i-1}\rho^{i-k_1-1}w^*(j)g_r[k_1]x(i) + \rho^{j-1}h_r[1]x^*(j)w(i) \\ &\quad \left. + \sqrt{1-\rho^2}\sum_{k_2=1}^{j-1}\rho^{j-k_2-1}w(i)g_r^*[k_2]x^*(j) + w(i)w^*(j)\right] \\ &= \sigma_h^2\left(\rho^{i+j-2} + (1-\rho^2)\sum_{k=1}^{\min(i,j)-1}\rho^{i+j-2k-2}\right)x(i)x^*(j) = \sigma_h^2\rho^{|j-i|}x(i)x^*(j),\end{aligned}$$

where (a) follows from zero valued conditional expectation of the signal samples.

Using the above derivations for the individual samples, the conditional expectation and variance of the mean Y of the signal samples can be evaluated as follows:

$$\begin{aligned}\mathbb{E}[Y] &= \mathbb{E}\left[\frac{1}{N}\sum_{n=1}^N y(n)\right] = \frac{1}{N^2}\left(\mathbb{E}\left[\sum_{n=1}^N y(n)\right]\right) = \frac{1}{N^2}\left(\sum_{n=1}^N \mathbb{E}[y(n)]\right) = 0, \\ \text{Var}[Y] &= \text{Var}\left[\frac{1}{N}\sum_{n=1}^N y(n)\right] = \frac{1}{N^2}\left(\sum_{n=1}^N \text{Var}[y(n)] + \sum_{n_1 \neq n_2} \text{Cov}[y(n_1), y(n_2)]\right) \\ &= \frac{1}{N^2}\left(\sigma_h^2\sum_{n=1}^N |x(n)|^2 + N\sigma_n^2 + \sigma_h^2\sum_{n_1 \neq n_2} \rho^{|n_1-n_2|}x(n_1)x^*(n_2)\right) = \frac{1}{N}(\sigma_h^2M_N + \sigma_n^2)\end{aligned}$$

$$\stackrel{(a)}{\approx} \frac{1}{N} (\sigma_h^2 \mathbb{E}[M_N] + \sigma_n^2) = \frac{1}{N} \left(\sigma_h^2 \mathbb{E}[|X|^2] + \frac{2\rho}{1-\rho} \left(1 - \frac{1-\rho^N}{N(1-\rho)}\right) |\mathbb{E}[X]|^2 + \sigma_n^2 \right), \quad (37)$$

where (a) results from the approximation of M_N by its expectation, given in Lemma 1.

C. Proof of Lemma 3

Observe that when conditioned on the ambient signal $x(n)$, the three signal components of the received signal under the alternate hypothesis \mathcal{H}_1 , given by (i) the direct signal from ambient source, (ii) the backscatter signal, and (iii) the receiver noise, are independent of each other.

$$y(n) = h_r(n)x(n) + \underbrace{\alpha h_b(n)h_t(n)x(n)}_{y_b(n)} + w(n) \quad (38)$$

This means that the expectation and variance of the sum can be derived using just the expectation and variance of each component. Since, we have already computed the expectation and variance of the direct signal and the receiver noise combination (in Lemma 3 for \mathcal{H}_0), it is now enough to compute the expectation and variance of the backscatter component $y_b(n)$.

To derive that, we further condition the signal on $h_b(n)$ since it will preserve and allow us to use the additive property of the Gaussian RVs. The conditional expectation and variance of an individual sample of the backscatter signal $y_b(n)$ and the conditional covariance of any two distinct samples $y(i)$ and $y(j)$ can be evaluated as:

$$\mathbb{E}[y_b(n)] = \mathbb{E}[\alpha h_b(n)h_t(n)x(n)] = \alpha h_b(n)x(n)\mathbb{E}[h_t(n)] = 0,$$

$$\text{Var}[y_b(n)] = \text{Var}[\alpha h_b(n)h_t(n)x(n)] = |\alpha|^2 |h_b(n)x(n)|^2 \text{Var}[h_t(n)] = |\alpha|^2 \sigma_h^2 |h_b(n)x(n)|^2,$$

$$\text{Cov}[y_b(i), y_b(j)] = |\alpha|^2 h_b(i)h_b^*(j)x(i)x^*(j) \text{Cov}[h_t(i), h_t(j)] = |\alpha|^2 \sigma_h^2 \rho^{|j-i|} h_b(i)h_b^*(j)x(i)x^*(j).$$

The conditional expectation and variance of the mean of signal samples $y_b(n)$ can be determined from their corresponding expectation and variance of the individual samples as follows:

$$\begin{aligned} \mathbb{E}\left[\frac{1}{N} \sum_{n=1}^N y_b(n)\right] &= \frac{1}{N^2} \left(\mathbb{E}\left[\sum_{n=1}^N y_b(n)\right] \right) = \frac{1}{N^2} \left(\sum_{n=1}^N \mathbb{E}[y_b(n)] \right) = 0, \\ \text{Var}\left[\frac{1}{N} \sum_{n=1}^N y_b(n)\right] &= \frac{1}{N^2} \left(\sum_{n=1}^N \text{Var}[y_b(n)] + \sum_{n_1 \neq n_2} \text{Cov}[y_b(n_1), y_b(n_2)] \right) \\ &= \frac{1}{N^2} \left(|\alpha|^2 \sigma_h^2 \sum_{n=1}^N |h_b(n)x(n)|^2 + |\alpha|^2 \sigma_h^2 \sum_{n_1 \neq n_2} \rho^{|n_1-n_2|} h_b(n_1)h_b^*(n_2)x(n_1)x^*(n_2) \right) \\ &= \frac{1}{N} |\alpha|^2 \sigma_h^2 \underbrace{\frac{1}{N} \sum_{1 \leq n_1, n_2 \leq N} \rho^{|n_1-n_2|} h_b(n_1)h_b^*(n_2)x(n_1)x^*(n_2)}_{M_N^b}. \end{aligned} \quad (39)$$

The sequence M_N^b , similar to M_N , is a function of the sum variable of the ambient sequence $x(n)$ and can be shown to asymptotically converge to its expectation. This expected value of M_N^b can be evaluated as follows:

$$\begin{aligned}
\mathbb{E}[M_N^b] &= \mathbb{E}\left[\frac{1}{N} \sum_{1 \leq n_1, n_2 \leq N} \rho^{|n_1-n_2|} h_b(n_1) h_b^*(n_2) x(n_1) x^*(n_2)\right] \\
&= \frac{1}{N} \mathbb{E}\left[\sum_{1 \leq n \leq N} |h_b(n)x(n)|^2 + \sum_{n_1 \neq n_2} \rho^{|n_1-n_2|} h_b(n_1) h_b^*(n_2) x(n_1) x^*(n_2)\right] \\
&= \frac{1}{N} \left(\sum_{1 \leq n \leq N} \mathbb{E}[|h_b(n)|^2] \mathbb{E}[|x(n)|^2] + \sum_{n_1 \neq n_2} \rho^{|n_1-n_2|} \mathbb{E}[h_b(n_1) h_b^*(n_2)] \mathbb{E}[x(n_1)] \mathbb{E}[x^*(n_2)] \right) \\
&\stackrel{(b)}{=} \frac{1}{N} \left(\sigma_h^2 \sum_{1 \leq n \leq N} \mathbb{E}[|X|^2] + \sigma_h^2 \sum_{n_1 \neq n_2} \rho^{2|n_1-n_2|} |\mathbb{E}[X]|^2 \right) \stackrel{(c)}{=} \sigma_h^2 \mathbb{E}[|X|^2] + \sigma_h^2 \frac{2\rho^2}{1-\rho^2} \left(1 - \frac{1-\rho^{2N}}{N(1-\rho^2)}\right) |\mathbb{E}[X]|^2,
\end{aligned}$$

where (b) follows from the assumption that the ambient sequence $x(n)$ is i.i.d. and the expectation of $h_b(n_1)h_b^*(n_2)$ which is given by $\sigma_h^2 \rho^{|n_1-n_2|}$, and (c) follows from the value of summation $\sum_{n_1 \neq n_2} \rho^{2|n_1-n_2|}$ that can be derived using (34) in Lemma 1.

The conditional variance of the mean of signal samples $y_b(n)$ can thus be approximated using the expectation of M_N^b which is given by:

$$\begin{aligned}
\text{Var}\left[\frac{1}{N} \sum_{n=1}^N y_b(n)\right] &\approx \frac{1}{N} (|\alpha|^2 \sigma_h^2 \mathbb{E}[M_N^b]) \\
&= \frac{1}{N} \left(|\alpha|^2 \sigma_h^4 \mathbb{E}[|X|^2] + |\alpha|^2 \sigma_h^4 \frac{2\rho^2}{1-\rho^2} \left(1 - \frac{1-\rho^{2N}}{N(1-\rho^2)}\right) |\mathbb{E}[X]|^2 \right). \quad (40)
\end{aligned}$$

The final step is to obtain the variance of mean Y of the signal samples under \mathcal{H}_1 by adding the individual variances in (37) and (40) respectively. This completes the proof.

D. Proof of Lemma 4

For the second scheme, the null hypothesis \mathcal{H}_0 corresponds to the scenario $b[0] \equiv 0$ and $b[1] \equiv 1$, and the alternate hypothesis \mathcal{H}_1 corresponds to the case $b[0] \equiv 1$ and $b[1] \equiv 0$. The respective marginal conditional distributions of the mean of the received signal samples $Y_{\mathcal{M}_2}[0]$ and $Y_{\mathcal{M}_2}[1]$ for the two symbol duration are given by:

$$\mathcal{H}_0 \begin{cases} Y_{\mathcal{M}_2}[0] \sim \mathcal{CN}(0, \text{Var}_0^{\text{SA}}) \\ Y_{\mathcal{M}_2}[1] \sim \mathcal{CN}(0, \text{Var}_1^{\text{SA}}), \end{cases} \quad \mathcal{H}_1 \begin{cases} Y_{\mathcal{M}_2}[0] \sim \mathcal{CN}(0, \text{Var}_1^{\text{SA}}) \\ Y_{\mathcal{M}_2}[1] \sim \mathcal{CN}(0, \text{Var}_0^{\text{SA}}). \end{cases} \quad (41)$$

Note that $Y_{\mathcal{M}_2}[0]$ and $Y_{\mathcal{M}_2}[1]$ are independent under each of the hypotheses. Therefore, the joint conditional distribution functions can be expressed as the product of the marginal conditional distributions which completes the proof.

E. Proof of Theorem 1

By comparing the conditional PDFs of the two hypotheses derived in Lemmas 2 and 3 respectively, the optimal decision rule of the first encoding scheme is given by:

$$\begin{aligned} \ln \left[f_{Y_{\mathcal{M}_1}|\mathcal{H}_0}(y) \right] &\gtrless_1^0 \ln \left[f_{Y_{\mathcal{M}_1}|\mathcal{H}_1}(y) \right] \\ -\ln(\text{Var}_0^{\text{SA}}) - \frac{|y|^2}{\text{Var}_0^{\text{SA}}} &\gtrless_1^0 -\ln(\text{Var}_1^{\text{SA}}) - \frac{|y|^2}{\text{Var}_1^{\text{SA}}} \\ |y|^2 &\gtrless_1^0 \ln \left(\frac{\text{Var}_1^{\text{SA}}}{\text{Var}_0^{\text{SA}}} \right) \frac{\text{Var}_1^{\text{SA}} \text{Var}_0^{\text{SA}}}{\text{Var}_1^{\text{SA}} - \text{Var}_0^{\text{SA}}}, \end{aligned} \quad (42)$$

where y is the mean of the signal samples received in the current slot under \mathcal{M}_0 . The optimal detection threshold $T_{\mathcal{M}_1}$ can be obtained from the decision rule in (42).

Observe that the decision rule is dependent on $|y|^2$ whose PDF is characterized by the exponential distribution. The mean of the exponential distribution is related to the variance of the complex Gaussian by the relation, $X \sim \mathcal{CN}(0, \sigma^2) \implies |X|^2 \sim \text{Exp}(\sigma^2)$. Assuming equal prior probabilities for the two hypotheses, the equation for the average BER is given by:

$$\begin{aligned} P_{\mathcal{M}_1}^{\text{SA}}(e) &= P(\mathcal{H}_0)P_{\mathcal{M}_1}^{\text{SA}}(e|\mathcal{H}_0) + P(\mathcal{H}_1)P_{\mathcal{M}_1}^{\text{SA}}(e|\mathcal{H}_1) \\ &= \frac{1}{2} \left(\Pr \{ |Y_{\mathcal{M}_1}|^2 > T_{\mathcal{M}_1} | \mathcal{H}_0 \} + \Pr \{ |Y_{\mathcal{M}_1}|^2 < T_{\mathcal{M}_1} | \mathcal{H}_1 \} \right) \\ &= \frac{1}{2} \left(1 - F_{\text{Exp}}(T_{\mathcal{M}_1}, \text{Var}_0^{\text{SA}}) + F_{\text{Exp}}(T_{\mathcal{M}_1}, \text{Var}_1^{\text{SA}}) \right) = \frac{1}{2} - \frac{1}{2} e^{-\frac{T_{\mathcal{M}_1}}{\text{Var}_1^{\text{SA}}}} + \frac{1}{2} e^{-\frac{T_{\mathcal{M}_1}}{\text{Var}_0^{\text{SA}}}}, \end{aligned}$$

where $F_{\text{Exp}}(x, \lambda) = 1 - e^{-\frac{x}{\lambda}}$ is the cumulative distribution function value of an exponential RV with mean λ at point x .

F. Proof of Theorem 2

By comparing the joint conditional distribution functions, evaluated in Lemma 4, the optimal decision rule of the encoding scheme \mathcal{M}_2 can be derived as follows:

$$\begin{aligned} \ln \left[f_{Y_{\mathcal{M}_2}[0], Y_{\mathcal{M}_2}[1]|\mathcal{H}_0}(y_0, y_1) \right] &\gtrless_1^0 \ln \left[f_{Y_{\mathcal{M}_2}[0], Y_{\mathcal{M}_2}[1]|\mathcal{H}_1}(y_0, y_1) \right] \\ -\frac{|y_0|^2}{\text{Var}_0^{\text{SA}}} - \frac{|y_1|^2}{\text{Var}_1^{\text{SA}}} &\gtrless_1^0 -\frac{|y_0|^2}{\text{Var}_1^{\text{SA}}} - \frac{|y_1|^2}{\text{Var}_0^{\text{SA}}} \end{aligned}$$

$$|y_0|^2 \gtrless_0^1 |y_1|^2. \quad (43)$$

Similar to the first scheme, the optimal decision rule of this scheme is dependent on $|y_0|^2$ and $|y_1|^2$ whose PDFs are given by exponential distributions. Due to the symmetry of the hypotheses, we only need to find error probability for hypothesis \mathcal{H}_0 . The expression for the theoretical average BER of \mathcal{M}_2 can be derived as follows:

$$\begin{aligned} P_{\mathcal{M}_2}(e) &= \Pr \{ |Y_{\mathcal{M}_2}[0]|^2 > |Y_{\mathcal{M}_2}[1]|^2 \mid \mathcal{H}_0 \} = \Pr \{ |Y_{\mathcal{M}_2}[0]|^2 > t \mid |Y_{\mathcal{M}_2}[1]|^2 = t, \mathcal{H}_0 \} \\ &= \int_0^{\infty} [1 - F_{\text{Exp}}(t, \text{Var}_0^{\text{SA}})] f_{\text{Exp}}(t, \text{Var}_1^{\text{SA}}) dt \\ &= \int_0^{\infty} e^{-\frac{t}{\text{Var}_0^{\text{SA}}}} \frac{e^{-\frac{t}{\text{Var}_1^{\text{SA}}}}}{\text{Var}_1^{\text{SA}}} dt = \int_0^{\infty} \frac{e^{-t\left(\frac{1}{\text{Var}_0^{\text{SA}}} + \frac{1}{\text{Var}_1^{\text{SA}}}\right)}}{\text{Var}_1^{\text{SA}}} dt = \left(1 + \frac{\text{Var}_1^{\text{SA}}}{\text{Var}_0^{\text{SA}}}\right)^{-1}, \end{aligned}$$

where $f_{\text{Exp}}(x, \lambda) = \frac{1}{\lambda} e^{-\frac{x}{\lambda}}$ is the PDF value of an exponential RV with mean λ at point x .

G. Proof of Lemma 5

The effective signal $y_{\text{eff}}(n)$ under \mathcal{H}_0 , given in (26), is the difference of two complex Gaussian RVs which again results in a complex Gaussian RV with variance equal to the sum of variances of the two individual RVs which computes to $2\sigma_n^2$. Hence, the mean Y of the received samples under \mathcal{H}_0 is a complex Gaussian RV with variance $\text{Var}_0^{\text{MA}} = \frac{2\sigma_n^2}{N}$. On the other hand, $y_{\text{eff}}(n)$ under \mathcal{H}_1 given in (27), is the sum of a scaled version of the backscatter signal $y_b(n)$ in Lemma 3 and the receiver noise with twice the variance. Using the procedure similar to the ones in Lemmas 2 and 3, the mean Y of the received samples under \mathcal{H}_1 can also be shown to follow a complex Gaussian distribution, the variance of which is given by

$$\text{Var}_1^{\text{MA}} = \frac{4 \sin^2\left(\frac{\phi_2 - \phi_1}{2}\right) |\alpha|^2 \sigma_h^4 \left\{ \mathbb{E}[|X|^2] + \frac{2\rho^2}{1-\rho^2} \left(1 - \frac{1-\rho^{2N}}{N(1-\rho^2)}\right) |\mathbb{E}[X]|^2 \right\} + 2\sigma_n^2}{N}.$$

H. Proof of Theorem 3

By comparing the conditional PDFs of the two hypotheses given in (28), the optimal detection threshold $T_{\mathcal{M}_1}$ of the scheme \mathcal{M}_1 can be obtained. The conditional BER is evaluated using a procedure similar to the one used for the average BER in case of a single antenna receiver. The average BER can be evaluated by marginalizing over the AoAs θ_1 and θ_2 .

For the second scheme \mathcal{M}_2 , the respective conditional distributions of the mean of the signal samples received for the two window slots $Y_{\mathcal{M}_2}[0]$ and $Y_{\mathcal{M}_2}[1]$ are given by:

$$\mathcal{H}_0 \begin{cases} Y_{\mathcal{M}_2}[0] \sim \mathcal{CN}(0, \text{Var}_0^{\text{MA}}) \\ Y_{\mathcal{M}_2}[1] \sim \mathcal{CN}(0, \text{Var}_1^{\text{MA}}), \end{cases} \quad \mathcal{H}_1 \begin{cases} Y_{\mathcal{M}_2}[0] \sim \mathcal{CN}(0, \text{Var}_1^{\text{MA}}) \\ Y_{\mathcal{M}_2}[1] \sim \mathcal{CN}(0, \text{Var}_0^{\text{MA}}). \end{cases} \quad (44)$$

The optimal decision rule after comparing the joint conditional distribution functions is again given by (43). The expression for conditional BER can be derived as follows:

$$\begin{aligned} P_{\mathcal{M}_2}(e|\phi_1, \phi_2) &= \left(1 + \frac{4 \sin^2\left(\frac{\phi_2 - \phi_1}{2}\right) |\alpha|^2 \sigma_h^4 \left\{ \mathbb{E}[|X|^2] + \frac{2\rho^2}{1-\rho^2} \left(1 - \frac{1-\rho^{2N}}{N(1-\rho^2)}\right) |\mathbb{E}[X]|^2 \right\} + 2\sigma_n^2}{2\sigma_n^2} \right)^{-1} \\ &= \frac{\sigma_n^2}{2 \left(\sin^2\left(\frac{\phi_2 - \phi_1}{2}\right) |\alpha|^2 \sigma_h^4 \left\{ \mathbb{E}[|X|^2] + \frac{2\rho^2}{1-\rho^2} \left(1 - \frac{1-\rho^{2N}}{N(1-\rho^2)}\right) |\mathbb{E}[X]|^2 \right\} + \sigma_n^2 \right)}. \end{aligned}$$

We can observe from the above expression that the conditional BER reaches zero at higher values of SNR. The above expression is dependent on the difference between the phase-offsets of the two links. To understand the average performance of the detection mechanism, we can average over the range of phase-offset values. For a linear uniform antenna array, the phase offset is related to AoA θ by the relation $\phi = \frac{2\pi}{\lambda} d \cos \theta$. The assumption is that the AoAs of direct link θ_1 and backscatter link θ_2 are identical, independent and uniformly distributed over the range $(-\pi, \pi]$. Marginalizing over the range of θ_1 and θ_2 , we get the expression in the result.

I. Estimation of phase offset of the direct path in time-selective fading

We can determine the phase-offset inversion component of the direct RF link at the receiver using the following approach. When message bit of value 0 is transmitted, the received signal at the two antenna elements is given by:

$$\mathbf{y}(n) = \begin{bmatrix} y_0(n) \\ y_1(n) \end{bmatrix} = h_r(n) \begin{bmatrix} 1 \\ e^{j\phi_1} \end{bmatrix} x(n) + \begin{bmatrix} w_0(n) \\ w_1(n) \end{bmatrix}. \quad (45)$$

Taking the summation over samples of block length N gives the following signal:

$$\sum_{n=1}^N \mathbf{y}(n) = \begin{bmatrix} \sum_{n=1}^N y_0(n) \\ \sum_{n=1}^N y_1(n) \end{bmatrix} = \sum_{n=1}^N h_r(n) x(n) \begin{bmatrix} 1 \\ e^{j\phi_1} \end{bmatrix} + \begin{bmatrix} \sum_{n=1}^N w_0(n) \\ \sum_{n=1}^N w_1(n) \end{bmatrix} = c_0 \begin{bmatrix} 1 \\ e^{j\phi_1} \end{bmatrix} + \begin{bmatrix} n_0 \\ n_1 \end{bmatrix}, \quad (46)$$

where $c_0 \sim \mathcal{CN}\left(0, N \left\{ \mathbb{E}[|X|^2] + \frac{2\rho}{1-\rho} \left(1 - \frac{1-\rho^N}{N(1-\rho)}\right) |\mathbb{E}[X]|^2 \right\} \sigma_h^2\right)$, $n_0 \sim \mathcal{CN}(0, N\sigma_n^2)$ and $n_1 \sim \mathcal{CN}(0, N\sigma_n^2)$ are independent Gaussian random signals.

Taking cross-correlation of $\sum_{n=1}^N y_0(n)$ and $\sum_{n=1}^N y_1(n)$, we get:

$$\begin{aligned} \mathbb{E} \left[\sum_{n=1}^N y_0(n) \sum_{n=1}^N y_1^*(n) \right] &= \mathbb{E} [|c_0|^2] e^{-j\phi_1} + \mathbb{E} [c_0 n_1^*] + \mathbb{E} [c_0^* e^{-j\phi_1} n_0] + \mathbb{E} [n_0 n_1^*] \\ &= N \left\{ \mathbb{E} [|X|^2] + \frac{2\rho}{1-\rho} \left(1 - \frac{1-\rho^N}{N(1-\rho)} \right) |\mathbb{E} [X]|^2 \right\} \sigma_h^2 e^{-j\phi_1} \\ \implies e^{-j\phi_1} &= \frac{\mathbb{E} [\sum y_0(n) \sum y_1^*(n)]}{N \left\{ \mathbb{E} [|X|^2] + \frac{2\rho}{1-\rho} \left(1 - \frac{1-\rho^N}{N(1-\rho)} \right) |\mathbb{E} [X]|^2 \right\} \sigma_h^2}. \end{aligned} \quad (47)$$

REFERENCES

- [1] J. K. Devineni and H. S. Dhillon, “Non-coherent signal detection and bit error rate for an ambient backscatter link under fast fading,” *Proc., IEEE Globecom*, Dec. 2019.
- [2] V. Liu, A. Parks, V. Talla, S. Gollakota, D. Wetherall, and J. R. Smith, “Ambient backscatter: Wireless communication out of thin air,” *Proc., ACM SIGCOMM*, Aug. 2013.
- [3] B. Kellogg, V. Talla, S. Gollakota, and J. R. Smith, “Passive Wi-Fi: Bringing low power to Wi-Fi transmissions,” *Symposium on NSDI*, vol. 16, pp. 151–164, Mar. 2016.
- [4] D. Bharadia, K. Joshi, M. Kotaru, and S. Katti, “BackFi: high throughput Wi-Fi backscatter,” *Proc., ACM SIGCOMM*, pp. 283–296, Aug. 2015.
- [5] H. S. Dhillon, H. Huang, and H. Viswanathan, “Wide-area wireless communication challenges for the internet of things,” *IEEE Commun. Mag.*, vol. 55, no. 2, pp. 168–174, Feb. 2017.
- [6] J. K. Devineni and H. S. Dhillon, “Ambient backscatter systems: Exact average bit error rate under fading channels,” *IEEE Trans. Green Commun. and Networking*, vol. 3, no. 1, pp. 11–25, Mar 2019.
- [7] K. Lu, G. Wang, F. Qu, and Z. Zhong, “Signal detection and BER analysis for RF-powered devices utilizing ambient backscatter,” *Proc., Intl. Conf. on Wireless Commun. & Sig. Proc. (WCSP)*, Oct. 2015.
- [8] G. Wang, F. Gao, Z. Dou, and C. Tellambura, “Uplink detection and BER analysis for ambient backscatter communication systems,” *Proc., IEEE Globecom*, Dec. 2015.
- [9] G. Wang, F. Gao, R. Fan, and C. Tellambura, “Ambient backscatter communication systems: Detection and performance analysis,” *IEEE Trans. Commun.*, vol. 64, no. 11, pp. 4836 – 4846, Nov. 2016.
- [10] J. Qian, F. Gao, G. Wang, S. Jin, and H. Zhu, “Semi-Coherent Detection and Performance Analysis for Ambient Backscatter System,” *IEEE Trans. Commun.*, vol. 65, no. 12, Dec. 2017.
- [11] ———, “Noncoherent Detections for Ambient Backscatter System,” *IEEE Trans. Wireless Commun.*, vol. 16, no. 3, Mar. 2017.
- [12] Y. Liu, Z. Zhong, G. Wang, and D. Hu, “Uplink detection and BER performance for wireless communication systems with ambient backscatter and multiple receiving antennas,” *Proc., Intl. Conf. on Commun. and Networking in China (ChinaCom)*, pp. 79 – 84, Aug. 2015.
- [13] T. Zeng, G. Wang, Y. Wang, Z. Zhong, and C. Tellambura, “Statistical Covariance Based Signal Detection for Ambient Backscatter Communication Systems,” *Proc., IEEE Veh. Technology Conf. (VTC)*, Sep. 2016.
- [14] G. Yang, Y.-C. Liang, and Y. P. Rui Zhang, “Modulation in the Air: Backscatter Communication over Ambient OFDM Carrier,” *IEEE Trans. Commun.*, vol. 66, no. 3, Mar. 2018.

- [15] M. A. El Mossallamy, M. Pan, R. Jäntti, K. G. Seddik, G. Y. Li, and Z. Han, “Noncoherent backscatter communications over ambient ofdm signals,” *IEEE Trans. Commun.*, 2019.
- [16] Q. Tao, C. Zhong, H. Lin, and Z. Zhang, “Symbol detection of ambient backscatter systems with manchester coding,” *IEEE Trans. Wireless Commun.*, vol. 17, no. 6, pp. 4028–4038, 2018.
- [17] Y. Liu, G. Wang, Z. Dou, and Z. Zhong, “New Coding and Detection Schemes for Ambient Backscatter Communication Systems,” *IEEE Access*, Mar. 2017.
- [18] W. Zhao, G. Wang, S. Atapattu, and B. Ai, “Blind channel estimation in ambient backscatter communication systems with multiple-antenna reader,” in *2018 IEEE/CIC Intl. Conf. on Commun. in China (ICCC)*, 2018, pp. 320–324.
- [19] H. Guo, Q. Zhang, D. Li, and Y.-C. Liang, “Noncoherent multiantenna receivers for cognitive backscatter system with multiple RF sources,” *arXiv preprint, arXiv:1808.04316*, 2018.
- [20] Q. Zhang, H. Guo, Y.-C. Liang, and X. Yuan, “Constellation learning-based signal detection for ambient backscatter communication systems,” *IEEE J. Sel. Areas Commun.*, vol. 37, no. 2, pp. 452–463, 2018.
- [21] H. Guo, Q. Zhang, S. Xiao, and Y.-C. Liang, “Exploiting multiple antennas for cognitive ambient backscatter communication,” *IEEE Internet of Things Journal*, vol. 6, no. 1, pp. 765–775, 2018.
- [22] D. Darsena, G. Gelli, and F. Verde, “Joint channel estimation, interference cancellation, and data detection for ambient backscatter communications,” in *2018 IEEE 19th Intl. Workshop on SPAWC*, 2018, pp. 1–5.
- [23] H. S. Dhillon and G. Caire, “Wireless backhaul networks: Capacity bound, scalability analysis and design guidelines,” *IEEE Trans. Wireless Commun.*, vol. 14, no. 11, pp. 6043–6056, 2015.
- [24] A. Adhikary, J. Nam, J.-Y. Ahn, and G. Caire, “Joint spatial division and multiplexing-the large-scale array regime,” *IEEE Trans. Information Theory*, vol. 59, no. 10, pp. 6441–6463, 2013.
- [25] A. Adhikary, E. Al Safadi, M. K. Samimi, R. Wang, G. Caire, T. S. Rappaport, and A. F. Molisch, “Joint spatial division and multiplexing for mm-wave channels,” *IEEE J. Sel. Areas Commun.*, vol. 32, no. 6, pp. 1239–1255, 2014.
- [26] A. Adhikary, H. S. Dhillon, and G. Caire, “Massive-mimo meets hetnet: Interference coordination through spatial blanking,” *IEEE J. Sel. Areas Commun.*, vol. 33, no. 6, pp. 1171–1186, 2015.
- [27] K. E. Baddour and N. C. Beaulieu, “Autoregressive modeling for fading channel simulation,” *IEEE Trans. Wireless Commun.*, vol. 4, no. 4, pp. 1650–1662, 2005.
- [28] Z. Liu, X. Ma, and G. B. Giannakis, “Space-time coding and kalman filtering for time-selective fading channels,” *IEEE Trans. Commun.*, vol. 50, no. 2, pp. 183–186, 2002.
- [29] C. Komminakis, C. Fragouli, A. H. Sayed, and R. D. Wesel, “Multi-input multi-output fading channel tracking and equalization using kalman estimation,” *IEEE Tran. on Signal Processing*, vol. 50, no. 5, pp. 1065–1076, 2002.
- [30] S. Ghandour-Haidar, L. Ros, and J.-M. Brossier, “On the use of first-order autoregressive modeling for rayleigh flat fading channel estimation with kalman filter,” *Signal Processing*, vol. 92, no. 2, pp. 601–606, 2012.
- [31] H. S. Wang and P.-C. Chang, “On verifying the first-order markovian assumption for a rayleigh fading channel model,” *IEEE Trans. Vehicular Technology*, vol. 45, no. 2, pp. 353–357, 1996.
- [32] F. Fuschini, C. Piersanti, F. Paolazzi, and G. Falciai, “Analytical approach to the backscattering from UHF RFID transponder,” *IEEE Antennas and Wireless Propagation Letters*, vol. 7, pp. 33–35, 2008.
- [33] C. A. Balanis, “Antenna theory: analysis and design, john willey and & son,” *New York*, 1997.
- [34] A. Bletsas, A. G. Dimitriou, and J. N. Sahalos, “Improving backscatter radio tag efficiency,” *IEEE Trans. Microwave Theory Tech*, vol. 58, no. 6, pp. 1502–1509, 2010.
- [35] D. Tse and P. Viswanath, “Fundamentals of wireless communication,” *Cambridge University Press*, 2005.